JGR Planets

RESEARCH ARTICLE
10.1029/2018JE005911

Key Points:
- Gas from Cl- and S-rich, OH-poor magma readily transports iron and alkalis
- Magmatic gas produces micron-sized crystals of molysite, halite, sylvite, hematite, maghemite, silica, pyrrhotite, pyrite, and native sulfur
- The surface deposits may react during cooling and hydration to produce secondary phases including iron oxychlorides and hematite

Correspondence to:
H. Nekvasil,
hanna.nekvasil@stonybrook.edu

Citation:
Nekvasil, H., DiFrancesco, N. J., Rogers, A. D., Coraor, A. E., & King, P. L. (2019). Vapor-deposited minerals contributed to the Martian surface during magmatic degassing. *Journal of Geophysical Research: Planets*, *124*, 1592–1617. https://doi.org/10.1029/2018JE005911

Received 27 DEC 2018
Accepted 6 MAY 2019
Accepted article online 20 MAY 2019
Published online 25 JUN 2019

Author Contributions:
Conceptualization: H. Nekvasil, A. D. Rogers, A. E. Coraor
Data curation: H. Nekvasil
Formal analysis: H. Nekvasil, A. E. Coraor, P. L. King
Funding acquisition: H. Nekvasil
Investigation: H. Nekvasil, N. J. DiFrancesco
Methodology: H. Nekvasil, A. E. Coraor
Project administration: H. Nekvasil
Resources: H. Nekvasil
Supervision: H. Nekvasil
Visualization: H. Nekvasil
Writing - original draft: H. Nekvasil, N. J. DiFrancesco, A. D. Rogers, P. L. King
Writing – review & editing: H. Nekvasil, N. J. DiFrancesco, A. D. Rogers, P. L. King

Vapor-Deposited Minerals Contributed to the Martian Surface During Magmatic Degassing

H. Nekvasil[1], N. J. DiFrancesco[2], A. D. Rogers[1], A. E. Coraor[3], and P. L. King[4]

[1]Department of Geosciences, Stony Brook University, Stony Brook, NY, USA, [2]Department of Atmospheric and Geological Sciences, SUNY Oswego, Oswego, NY, USA, [3]Institute for Molecular Engineering, The University of Chicago, Chicago, IL, USA, [4]Research School of Earth Sciences, The Australian National University, Canberra, ACT, Australia

Abstract Martian magmas were likely enriched in S and Cl with respect to H_2O. Exsolution of a vapor phase from these magmas and ascent of the gas bubbles through the magma plumbing system would have given rise to shallow magmas that were gas-charged. Release and cooling of this gas from lava flows during eruption may have resulted in the addition of a significant amount of vapor-deposited phases to the fines of the surface. Experiments were conducted to simulate degassing of gas-charged lava flows and shallow intrusions in order to determine the nature of vapor-deposited phases that may form through this process. The results indicate that magmatic gas may have contributed a large amount of Fe, S, and Cl to the Martian surface through the deposition of iron oxides (magnetite, maghemite, and hematite), chlorides (molysite, halite, and sylvite), sulfur, and sulfides (pyrrhotite and pyrite). Primary magmatic vapor-deposited minerals may react during cooling to form a variety of secondary products, including iron oxychloride (FeOCl), akaganéite ($Fe^{3+}O$ (OH,Cl)), and jarosite ($KFe^{3+}{}_3(OH)_6(SO_4)_2$). Vapor-deposition does not transport significant amounts of Ca, Al, or Mg from the magma and hence, this process does not directly deposit Ca- or Mg-sulfates.

Plain Language Summary The surface of Mars is covered by dust, and this dust will be the most abundant material encountered by future manned missions to the planet's surface. Understanding the mineralogic makeup of this dust is vital to assessing its potential toxicity. This dust also records information on the most recent geological activity and atmospheric conditions on Mars. This work focuses on the potential contribution of micron-sized particles formed by condensation of gas from young lava flows to the dust. We experimentally simulated a boiling magma and exposed the gas given off to the temperatures that you might see above a lava flow. The results indicate that some of the minerals found in the fine-grained material of the Martian surface such as chlorides, sulfides, sulfur, and silica could be formed in this way. These precipitated minerals, in turn, can react with the cooling gas or the atmosphere to form a set of secondary minerals, such as maghemite and hematite, and very reactive substances such as iron oxychloride. Iron oxychloride can obliterate traces of the organic material that we have counted on to provide information about organics brought to Mars by meteorites and about potential past life on the planet.

1. Introduction

1.1. Occurrence of S and Cl on the Martian Surface

Chlorine and sulfur have been recognized as major components of Martian surface materials since Viking lander measurements of the regolith (e.g., Baird et al., 1976; Clark et al., 1977, 1982; Clark & Baird, 1979). Subsequent rovers with the Pathfinder, the Mars Exploration Rover (MER), and Mars Science Laboratory (MSL) missions and the Phoenix lander confirmed these observations (Franz et al., 2018; Gaillard et al., 2013; reviews in King & McLennan, 2010), even noting veins of sulfur-rich material containing up to 40 wt% S (Nachon et al., 2014). In situ measurements of the regolith by the instrument suites on board the MSL and MER rovers plus remote infrared and gamma ray spectra from orbit suggest that sulfur is hosted specifically by Mg-, Fe-, and Ca-sulfates (such as anhydrite), as well as pyrite, pyrrhotite, jarosite, and minor amounts of other sulfates, sulfides, and native sulfur (review in Franz et al., 2018).

Orbiter data suggest that the Cl concentration of the Martian surface ranges from approximately 0.1 to 1 wt% with an average of 0.49 wt% globally (Keller et al., 2006). Elevated chlorine concentrations of the Martian surface have also been confirmed by all rover and lander missions (Clark & Van Hart, 1981; Gellert et al., 2004, 2006; Hecht et al., 2009; McLennan et al., 2014; Wänke et al., 2001). The Cl content of Martian dust

and soil compositions from the alpha-particle x-ray spectrometer and mass spectrometry using the Sample Analysis at Mars (SAM) instrument (Berger et al., 2016; Glavin et al., 2013) are in general agreement with the orbiter data. The abundant chlorine on the Martian surface is hosted in reduced chlorides and oxidized chlorates and perchlorates. THEMIS data indicate that Cl is in part hosted by halite and possibly other chlorides such as sylvite and molysite in playa-like deposits on Mars (Osterloo et al., 2008, 2010); for example, Glotch et al. (2016) suggest that halite may comprise up to 25% of the fines in these regions. Chlorine is also hosted by perchlorate salts in the regolith of Mars' North Pole investigated by the Phoenix Mars Lander (Hecht et al., 2009; Kounaves et al., 2014) and in the Rocknest fines at Gale Crater by MSL (Glavin et al., 2013).

Commonly considered mechanisms for the formation of the sulfates and chlorides/perchlorates in Martian fine-grained material involve secondary processes acting upon preexisting sulfide- and chloride-bearing bedrock sources. Studies of igneous Martian meteorites indicate that these rocks contain primary igneous sulfides, predominantly pyrrhotite (see review of King & McLennan, 2010), and Cl-bearing minerals, such as amphiboles (e.g., Giesting & Filiberto, 2016; Johnson et al., 1991), Cl-scapolite (Filiberto et al., 2014), and apatite (e.g., McCubbin & Nekvasil, 2008; Righter et al., 2002). Oxidation of primary sulfide minerals to form sulfates is speculated to have occurred through water-rock or ice-rock interaction (Bibring et al., 2006; Burns & Fisher, 1990; Chevrier & Mathé, 2007; King et al., 2004; King & McSween, 2005; McCollom & Hynek, 2005; Niles & Michalski, 2009; Yant et al., 2016). Sulfate dispersion into Martian fines would then have resulted from mechanical erosion of these secondary sulfates, dissolution, and possible transport in fluvial systems, followed by evaporation of surface waters before aeolian transport. Martian chloride deposits are also considered to be secondary in nature, with aqueous dissolution of Cl from an original chloride-bearing bedrock followed by evaporation either in situ (Osterloo et al., 2008, 2010) or after significant transport to lake beds and deltaic regions (e.g., Hynek et al., 2015).

Secondary processes such as alteration, erosion, and transport of bedrock sulfides and chlorides undoubtedly remobilized Cl and S to the Martian regolith. However, it has been long recognized that magmatic gas also has a significant role in adding S and halogens to the surface (e.g., Clark & Van Hart, 1981; King & McSween, 2005; Settle, 1979; Ustunisik et al., 2011) and can produce both primary vapor-deposited minerals and secondary minerals through interaction with the surface. While much effort has gone into exploring sedimentological processes that contributed to the enrichment of these elements in Martian fines, less is known about the role of magmatic vapors in forming halogen- and sulfur-bearing minerals (Gooding, 1978; Gooding et al., 1992).

1.2. Contributions of Magmatic Gas to the Martian Surface

On Earth, magmatic gas released during major explosive eruptions is considered to be a primary contributor of H_2O, and C-, S-, and Cl-bearing gaseous species to the atmosphere. Large explosive eruptions on Mars that formed the paterae and blanketed the planet with a variety of pyroclastic deposits (e.g., Wilson & Head, 2007) likely also primarily contributed gaseous species such as H_2O, SO_2, HCl, S, and H_2S to the atmosphere, with SO_2 dominating as a primary magmatic gaseous species (Gaillard & Scaillet, 2009; Symonds et al., 1994) and as a secondary species produced by reaction of H_2S in the Martian atmosphere (e.g., Bluth et al., 1995). Such large explosive eruptions are commonly called upon to account for widespread aerosol sulfate production through both wet and dry processes on Earth and on Mars (e.g., Settle, 1979). However, persistent quiescent degassing from lava flows, small-scale fire-fountaining, shallow magma bodies, and small fumaroles, commonly referred to as "open-vent" or "passive" degassing, could have been a significant source of more locally distributed magmatic gas during the late stages of Martian volcanism as large explosive eruptions decreased in frequency and effusive volcanism from shield-building magmatism became more common. In fact, even for Earth, where explosive eruptions occurs with great regularity, the time-averaged gaseous emissions from passive degassing is greater than from less common explosive events (Mather et al., 2003).

Shallow degassing as a significant source of magmatic gas appears inconsistent with the low volatile solubilities in low-pressure magma, as low volatile solubility would imply that only an insignificant amount of gas would be released by exsolution from a cooling lava flow. However, it has been proposed that gas from deeper portions of the magma plumbing can become concentrated in shallow regions—a process invoked to explain the "excess S" problem on Earth (Henley & Seward, 2018; Shinohara, 2008; Wallace, 2001)—and

loss of this entrained gas during quiescent volcanism would contribute more magmatic gas to the Martian surface than could be provided solely by low-pressure exsolution of gas from the erupted lava. This process has also been called upon to concentrate H_2O-CO_2-Cl-S-bearing gases (e.g., Johnson et al., 2010). Localized degassing and cooling of the gas released from passive magmatism would result in a smaller contribution of magmatic gas to the upper atmosphere and larger contribution to the local surface through the formation of vapor-deposited solids.

Our understanding of the nature of volcanic gas sublimates and their stability temperatures has been greatly aided by direct observation of sublimate production on Earth. Silica glass tubes positioned inside small fumaroles allow for the concentration of vapor and the collection of precipitated mineral phases forming along the inner walls of the tube (e.g., Africano et al., 2002; Bernard & Le Guern, 1986; Taran et al., 1995; Yudovskaya et al., 2008; Zelenski et al., 2013). Analysis of sublimates forming from gas emitted at high-temperature vents from the potential Martian analog shield volcano Erte Ale (on the East African rift, Benoit et al., 2006; de Moor et al., 2013) shows a high-to-low temperature sequence of oxides, silicates, platinum group elements, sulfides, sulfates, halides, fluorosilicates, and native sulfur (Zelenski et al., 2013). The most abundant sublimate minerals observed were Fe/Ti oxides, silicates, halite, sylvite, amorphous silica, native sulfur, and trace metal-sulfides/chlorides (Zelenski et al., 2013).

It is not known how well terrestrial magmatic vapor-deposited material reflects the vapor-deposited minerals produced on Mars during passive degassing since the compositions of volcanic gas and the subsequently vapor-deposited minerals are dependent on the composition and the volatile load of the parental magma/lava from which the gases were exsolved (e.g., Renggli et al., 2017). The possibility of significant differences between the dissolved volatile load of Martian magmas and terrestrial magmas has been recognized. S-bearing gaseous species may have been more abundant in Martian volcanic gases due to a higher S content of the Martian mantle. In fact, Gaillard and Scaillet (2009) concluded that up to 50 mol% of the post 4.5-Ga Martian volcanic gases could have been composed of S-species. A lower water content of the Martian mantle and primary melts has been suggested based on petrologic evidence (e.g., Filiberto, Baratoux, et al., 2016; Filiberto, Gross, et al., 2016; Kiefer et al., 2015; McCubbin et al., 2016). Also, Filiberto, Gross, et al., 2016 (and references within) suggested that halogen concentrations in the Martian mantle were as much as three times greater than what is found in the terrestrial mantle. Adding to the potential of significantly higher Cl/H_2O ratios of primitive Martian magmas compared to primary terrestrial magmas is the possibility of greater mantle dehydration relative to Cl-depletion induced by successive partial melting (due to the greater retention of Cl relative to H in mantle minerals during high temperature melting, cf. Aubaud et al., 2004, Joachim et al., 2015).

In view of the strong possibility that terrestrial fumarolic gases may not be analogous to low-OH Martian magmatic gases, the use of thermodynamic models of vapor/sublimate mineral equilibria is a reasonable first-line approach to assessing the nature of Martian vapor-deposited mineral since they allow for compositional variability of the bulk gas composition. Model prediction of such equilibria based on thermodynamic properties of a variety of species from databases such as GASTHERM (Symonds & Reed, 1993) and JANAF (Chase, 1998) has evolved from the early work by Krauskopf (1957). A variety of software tools have been developed that incorporate an increasing number of chemical species in the vapor (e.g., HSC by Outotec). As summarized by Pokrovski et al. (2013), these calculations have had varied success in predicting sublimate chemistry of natural systems when compared to fumarole analysis in silica glass tubes. Three problems with such comparisons can be readily envisioned. First, the bulk gas composition, needed for any thermodynamic modeling, is a property that remains elusive in many natural fumaroles; this is even more the case for Mars. Second, equilibrium thermodynamics may not be applicable in a regime of high thermal gradient such as above a lava flow (e.g., Patrick et al., 2004), where thermodiffusion (Soret diffusion) can induce heterogeneous gas compositions over this gradient even for an originally homogeneous vapor. Finally, degassing lava flows or shallow magma bodies have a dispersed gas source (the lava itself), and during cooling, superposition of high and low temperature phases can be expected to occur across the surface of a flow. Importantly, this superposition will allow for reactions among previously precipitated phases during cooling that may lead to the formation of secondary minerals not predicted by thermodynamic sublimation modeling. For these reasons, we have elected to follow an experimental approach toward investigating the nature of vapor deposited material that could have been added to the Martian surface by passive degassing of OH-poor magma.

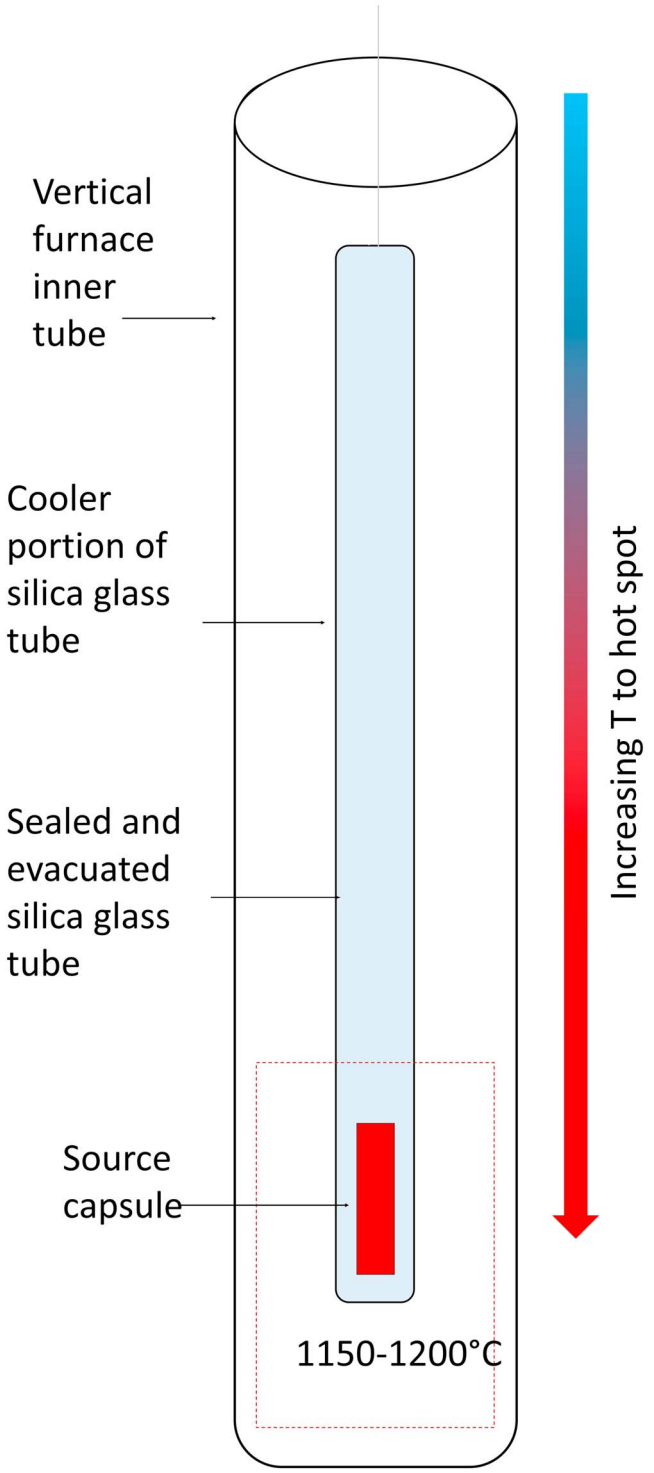

Figure 1. Schematic of experimental setup. A crimped $Au_{80}Pd_{20}$ capsule containing the source material lies at the bottom of a 28cm-long evacuated and sealed silica glass tube. The tube is placed in a strong thermal gradient inside of a Pt-wound furnace (not shown) such that the source is at the hot spot.

2. Experimental Design

Experiments attempted to simulate the natural cooling of magmatic gas proximal to a lava flow or in a small fire fountain, a gas whose multicomponent composition is initially dictated by the magma it was in equilibrium with and then modified due to thermodiffusion and precipitation of vapor-deposited minerals. Furthermore, these experiments emulated the mixing of high- and low-temperature vapor-deposited phases and the reactions among them as the local gas column cools.

The experiments were designed to (i) generate an oxidized magmatic froth that simulates a gas bubble-charged shallow magma in which the gas has equilibrated with an oxidized crust, (ii) allow this gas to separate from the silicate melt and ascend into an overlying cooler gas column in a strong thermal gradient, (iii) enable the formation and collection of solid vapor-deposited phases, and (iv) cool the gas column in order to permit reaction among previously precipitated phases.

The physical design of all experiments was modified from that of Ustunisik et al. (2011, 2015) and involved synthesis of a volatile-doped glass of basaltic composition (referred to here as the vapor "source") at elevated pressure (required to dissolve appropriate amounts of Cl and S). This source was then placed in a crimped capsule (sealed at the bottom) at the bottom of a long silica glass tube. The silica tube was evacuated, sealed, and placed in a vertically held furnace such that the capsule was at the hot spot and below a strong thermal gradient. This setup allowed the volatile-oversaturated source to melt and boil at low pressure, producing a high gas to melt ratio, forcing the gas out of the crimped capsule and into the tube. The vapor was trapped in the glass tube, which allowed deposits to form as the gas cooled in the thermal gradient of the overlying column (Figure 1). In many ways, these experiments simulate the glass tube fumarolic gas sampling technique used by workers such as Zelenski et al. (2013).

Assessment of the experimental technique was aided by additional experiments designed to (i) provide ground state information on whether crystalline vapor-deposited phases would form in the absence of Cl and S, (ii) determine if the temperature of the source affected the compositional types of vapor deposited phases produced, (iii) determine if the structural state of the source affected the nature of the vapor-deposited minerals produced, and (iv) whether the redox state of the source at the hot spot changed during the experiment.

2.1. Source Material Composition

Considering the likelihood that source composition plays a role in the nature of vapor-deposited minerals produced, a Martian rock composition, specifically, the alpha-particle x-ray spectrometer-analyzed "soil-corrected" composition of the Gusev Crater rock "Irvine" (McSween et al., 2006), was chosen to provide the magmatic froth. Irvine, a member of the Irvine-class rocks, was discovered in the Columbia Hills of Gusev Crater in a small sublinear outcrop, suggestive of an igneous dike. It has an aphanitic texture indicative of rapid crystallization and thus, is likely an igneous rock that has retained the composition of the magma from which it formed. Mini-TES and Mössbauer data indicate a modal mineralogy consisting of predominantly feldspar and pyroxene, Fe-Ti-oxides, and minor olivine and apatite (McSween et al., 2006), that is, a typical basaltic assemblage with little alteration (Morris et al., 2006).

Table 1
Chemical Composition of the Martian Rock Irvine and Electron Microprobe Analyses of Synthetic Source Glasses

Oxide	Mars bulk crust[a]	Irvine unbrushed[b]	Soil-corrected Irvine[b]	Volatile-free Irvine	I(NVA)[c] (11)[d]	1σ[e]	I(Cl+S)[f] (8)	1σ	I(Cl+HiS)[g]
SiO_2	49.01	45.98	46.94	47.30	48.90	0.16	48.73	0.35	47.03
TiO_2	0.95	1.04	1.06	1.07	1.13	0.01	1.00	0.04	1.05
Al_2O_3	10.30	10.37	10.58	10.66	8.96	0.04	11.23	0.22	10.01
FeO_T[h]	18.80	18.79	19.19	19.34	20.72	0.21	17.59	0.30	19.97
MnO	0.34	0.35	0.36	0.37	0.40	0.02	0.32	0.03	0.32
MgO	9.13	10.37	10.58	10.66	9.75	0.08	8.92	0.41	8.86
CaO	6.82	5.90	6.02	6.07	5.99	0.04	5.33	0.05	5.39
Na_2O	2.86	2.62	2.68	2.70	2.33	0.28	2.09	0.17	2.07
K_2O	0.48	0.67	0.67	0.68	0.58	0.05	0.53	0.03	0.56
P_2O_5	0.90	0.95	0.97	0.97	0.90	0.03	0.94	0.04	0.91
Cr_2O_3	0.40	0.20	0.20	0.20	0.24	0.01	0.17	0.01	0.16
SO_3	-	2.32	0.76	0.00	0.02	0.01	0.61	0.13	2.38
Cl	-	0.44	0.00	0.00	0.06	0.01	2.54	0.23	1.30

[a]Hahn and McLennan (2010). [b]McSween et al. (2006). [c]S- and Cl- free Irvine. [d]Number of analyses. [e]1σ standard deviations listed for samples analyzed by electron microprobe. [f]Synthetic Irvine with added Cl and S. [g]I(Cl+S) with added crystalline products from quenched S-rich co-existing immiscible melt from high pressure glass synthesis. [h]All Fe as FeO.

Chemical analysis showed that Irvine is a mildly alkalic basalt (McSween et al., 2006) with a composition similar to the bulk Martian crust (Hahn & McLennan, 2010). The Irvine composition contains both S and Cl. Although much of this is attributed to contamination by surface dust (McSween et al., 2006), it should be noted that the S content reported for this unbrushed rock (2.4 wt% SO_3 or 1 wt% S) is not an unreasonable S content of an oxidized basalt at sulfide saturation (Jugo et al., 2010).

2.2. Volatile Load of the Source

In order to ensure a high gas content for the experiment, a high gas/silicate melt ratio in the magmatic froth was required. Toward this end, the source synthesis capitalized on the higher volatile solubility at higher pressure. The Irvine composition synthesized was doped with S and Cl to levels higher than their likely magma concentrations at low pressure. This was purely to produce a source glass that was supersaturated in volatiles at low pressure. This supersaturation enabled the source to boil at low pressure and form the froth, thus simulating the magmatic froth produced by gas bubble concentration in the shallow reaches of a magma plumbing system. Whether the gas was concentrated in nature by ascent into shallow reaches of the magma plumbing system, or exsolved due to supersaturation at low pressure as is the case for the experiments, the final gas would be in equilibrium with the low-pressure silicate melt.

Using as a starting point the bulk chemical composition of the "soil-corrected" Irvine where the majority of S and Cl was computationally removed (McSween et al., 2006), the effect of volatile ratio, specifically S/Cl, was investigated by synthesizing two volatile-bearing compositions in addition to a Cl- and S-free composition (listed in Table 1 as no volatiles added "NVA" experiments). The presence of both Cl and S in each of the halogen-bearing source compositions ensured that the expected competition for coordinating ligands between the two anions was preserved. Based on the S solubility inferred by Gaillard and Scaillet (2009), the high S composition synthesized was anticipated to exsolve an immiscible sulfide liquid during high-pressure synthesis, which would crystallize during quench. Inclusion of this sulfide phase with the silicate glass as the source ensured a higher S budget of the source than the glass alone. The concentration of Cl for our Cl-bearing sources is ~3-5 times greater than observed in Irvine, again with the goal of producing a sufficient amount of gas-charged silicate froth and simulating a gas+ silicate melt assemblage at low pressure that is enriched in gas from bubble ascent. Although natural systems can concentrate a large amount of gas, the amount of gas we could produce experimentally was limited by the solubility of Cl at our synthesis pressure.

2.3. Redox State of the Source

The oxygen fugacity of the source material will affect the nature of the vapor-deposited minerals produced and therefore deserves special consideration in the experimental design. In spite of its apparent lack of alteration, the rock Irvine has a $Fe^{3+}/\Sigma Fe$ of 0.36, as determined though Mössbauer spectroscopy and

estimates of igneous mineral composition (Schmidt et al., 2013). This high degree of oxidation has been attributed at least in part to the oxidized dust layer (McSween, 1994). However, Schmidt et al. (2013), in their reevaluation of the oxygen fugacities of the igneous minerals in several Martian basalts, inferred oxygen fugacities for Irvine near QFM. While this corresponds to a more oxidized state than was originally accepted for Martian basalts (e.g., Herd et al., 2001; Herd, 2006), a wide diversity of oxygen fugacities has been reported for these basalts. Oxygen fugacity estimates range from values suggestive of IW to the NNO buffer (Herd, 2006; McSween, 1994; Santos et al., 2015; Schmidt et al., 2013). Not all of the higher oxidation states observed can be explained by weathering processes, suggesting that they may be magmatic (e.g., Santos et al., 2015). Herd et al. (2001), Herd (2006) and Wadhwa (2008) suggested that some of this oxidation occurred in the magmatic state after exposure to, or mixing with, more oxidized materials or magmas in the crust. This relatively high oxygen fugacity is similar to values for the augite basalt/shergottite NWA 8159 (Herd et al., 2017) that began crystallizing near or just below FMQ, with a later increase in oxygen fugacity to approximately 2 log units above FMQ. Since (i) Irvine appears to show minerals consistent with FMQ or slightly higher (Schmidt et al., 2013), (ii) there is clear evidence that Martian magmas can become oxidized when ascending to shallow levels, and (iii) oxidation of entrained gas should be readily attained during exposure to oxidized crust, we have chosen to investigate degassing of a magma of Irvine composition at an oxidation state intermediate between that of the magma and that of the surface, specifically, close to the NNO buffer. In this way we can provide information on the oxidized vapor deposited assemblage.

The late changes in oxygen fugacity in the igneous assemblage of some Martian rocks attests to the absence of an oxygen buffering assemblage in at least some Martian magmas at shallow levels. For this reason, the experiments were designed without an oxygen buffering assemblage. Instead, the ferrous/ferric ratio was set to be that of NNO at 1150°C in the starting source material. The value of this initial ratio was obtained by using the Irvine composition for a MELTS analysis (Ghiorso & Sack, 1995) of the effect of log (fO_2/1 bar; that is, log fugacity of oxygen relative to a 1 bar standard state) on the melt Fe^{3+}/Fe^{2+}ratio.

Considering the uncertainty of the computational models employed (which led to the computed ferric/ferrous ratio used), weighing uncertainty of the Fe sources, and potential for the oxygen fugacity of the molten source to change during the experiment (e.g., through oxidation of the melt caused by reduction of ferrous iron to Fe° in the melt and alloying of this metallic Fe to the $Au_{80}Pd_{20}$ capsule), an independent measure of the oxygen fugacity at the source was desired. To do this, we ran additional experiments that included a two-oxide oxygen monitor (Buddington & Lindsley, 1964). For this monitoring, the compositions of a two-oxide pair (an ilmenite-hematite solid solution and an ulvöspinel-magnetite solid solution) in equilibrium at 1150°C at the oxygen fugacity of the NNO buffer were computed using the thermodynamic model QUIlF (Andersen et al., 1993) and the value of the oxygen fugacity from the above MELTS analysis. A further calculation yielded an oxide pair that lay at slightly more oxidizing conditions. By using the "off-composition" pair, any compositional change would ascertain that the monitor was not acting as a buffer, and the direction of compositional change would constrain the redox state of the source while melted. This oxide pair was included in a separate capsule alongside the source-bearing capsule at the hot spot for two experiments, one using the I(NVA) and the other the I(Cl+S) source. To further enhance the possibility that the monitor did not act as a buffer, the weight ratio of monitor oxide to source was minimized. These oxides were reanalyzed after the experiments to determine if they changed composition during the experiment.

2.4. Structural State of the Source

Ideally in the laboratory, magma could be rapidly decompressed from elevated pressure to the low pressure of the degassing experiments while still in the molten state. In the absence of this capability, the use of quenched glass is a common alternative. However, some volatile compounds may be lost from the source glass during heating in the silica glass tube while the temperature is still below the glass transition temperature, that is, while in a thermal regime where the structural state and likely the binding energy of the volatile species may differ from that in a melt. In order to assess the sensitivity of the vapor-deposited minerals to loss of vapor before melting, we ran several parallel experiments using the reagent mixture of oxide components itself (e.g., the same mix that was used to synthesize the glass at high pressure). This starting material most likely would lose volatiles sequentially (due to decomposition of individual components of the mixture). If the vapor-deposited phases are the same for these very different source types and

bonding environments, it is likely that even though the loss of gas from the glass before melting is possible, the experiments may still provide information on vapor-deposited material produced directly by a cooling magma and we can be more confident that the simulated degassing information can be applied to natural systems.

3. Experimental Details

Powdered components (oxides, silicates, and sulfate) of the source magma were mixed together in ethanol and homogenized in automatic agate mortars for approximately 4 hr. Fe° sponge (needed for combination with hematite to provide the desired ferrous/ferric ratio) and $MgCl_2$ (for the chlorine-bearing sources) were added in the last hour to mitigate any oxidation or dissolution of the components, respectively. The $Fe^{2+}/(Fe^{2+}+Fe^{3+})$ ratio of this mixture was determined by the MELTS (Ghiorso & Sack, 1995) analysis mentioned above. This analysis indicated that a log (fO_2/1 bar) of -7 (~0.2 log units above NNO) at 1150°C would be achieved by setting the $Fe^{2+}/(Fe^{2+}+Fe^{3+})$ ratio of the synthetic source mixture to 0.8. For the I(Cl+S) mixture (Table 1), Cl and S were added as $MgCl_2$ and $Mg(SO_4)$, with the remaining Mg added as periclase to yield 2.5 wt % Cl, and 0.6 wt % SO_3 equivalent. The high-sulfur source mixture (I(Cl+HiS) of Table 1) was produced by adding an additional amount of pyrite + Fe° (with troilite stoichiometry) to the I(Cl+S) mix. Importantly, the variable oxidation state of the S added to the mixtures likely contributed little to the overall oxidation state of the mix, as the quantities of the S-bearing materials used was much lower the total Fe in the system (for which the redox state was set). The I(NVA) composition of Table 1 was made using only MgO (periclase) as the Mg source.

Glass of the source magma composition was produced by placing aliquots of the mix powder into Fe-soaked platinum capsules. These capsules were made by lining Pt capsules with (0.03 mm thick) Fe° foil and heating them to 1200°C under vacuum for 6 hr to allow the metals to alloy (with the hope of minimizing Fe-loss from our sample during glass synthesis). The capsules were loaded with the reagent mixture and then dried at 150°C in a vacuum oven for 12 hr, welded shut, and inserted into a talc cell containing a graphite furnace. Mullite spacers above and below the capsule ensured that it would be held at the hot spot in the pressure vessel. The assemblage was placed in a ¾ inch (19.13 mm) pressure vessel and inserted into a piston-cylinder press. The source mixtures were melted at 0.5 GPa, and 1300°C for 3 hr, after which the charge was rapidly quenched (~500 °C/min). Quenching produced a homogenous silicate glass or a silicate glass + quenched immiscible sulfide melt as determined by electron microprobe analysis performed at the American Museum of Natural History using a Cameca SX-100 microprobe. A 10-μm spot size, accelerating voltage 20kV, and beam current of 15 mA was employed, with an analysis time of 20-30 s per element. The following minerals were used for standardization: McKee jadeite, Na; potassium feldspar, K; San Carlos olivine, Mg; Wakefield plagioclase, Si and Ca; apatite, P; barite, S; Scapolite, Cl; ilmenite, Ti; $MgCr_2O_4$, Cr; rhodonite, Mn; and Rockport fayalite, Fe. Table 1 gives the electron microprobe analyses of the synthetic glass. Micro-Fourier transform infrared analysis of water content using the techniques of Dixon et al. (1995) and Mandeville et al. (2002) indicates that the source glasses additionally contained 0.4±0.2 wt% water; this uncertainty reflects the combination of the uncertainty induced by thickness variation of individual glass wafers and the overall variability of different aliquots of glass.

For the degassing experiments, the source glass (~150 mg) was loaded into $Au_{80}Pd_{20}$ capsules that were then loosely crimped and placed at the bottom of an ~28-cm-long silica glass tube (with a 7-mm inner diameter) that was sealed at the bottom. The tube was evacuated, sealed (by heating the open end with an oxygen torch, while the tube was still attached to the vacuum pump), and suspended in a vertical Pt-wound furnace with a thermal gradient such that the sample was in the hot spot and the lowest temperature of the tube was at ~200°C. Insertion of the tube was done over 20 min into the preheated furnace, and the temperature of the hot spot was rapidly reattained once the tube was fully inserted. For the parallel experiments investigating the effect of directly using the reagent mixture on the nature of the vapor-deposited material, mixes were loaded into an $Au_{80}Pd_{20}$ capsule and dried in a vacuum oven at 150°C for 12 hr before inserting into a silica glass tube and heating under the same conditions as the glass source. For each experiment, the tubes were heated for 12 to 96 hr with the source at either 1150° or 1200°C. After the experiment, the tube was removed from the furnace and hung in air to cool to room temperature.

For the experiments containing a 2-oxide oxygen monitor at 1150 °C, we chose an oxide pair, $Ilm_{72}Hm_{28}$ and $Usp_{48}Mt_{52}$ (kindly donated by D.H. Lindsley) that reflected an oxygen fugacity of NNO+0.6 log units, that is 0.6 log units above the oxygen fugacity preset by the $Fe^{2+}/(Fe^{2+}+Fe^{3+})$ of the source composition. The oxide pair was powdered, mixed in a 1:1 ratio, and X-rayed (to verify the compositions using the cell parameters and the variation of cell dimensions with changing composition of the solid solutions as per Lindsley, 1976). In order to minimize the chances that the monitor assemblage itself acted as a buffer, the amount of the oxide monitor loaded was about 0.2 times that of the source. [Although less monitor would be desirable, we had to ensure that sufficient monitor would be present for a definitive powder X-ray diffraction (PXRD) pattern of the oxide mixture after the experiment.] The oxide mixture was loaded into an $Au_{80}Pd_{20}$ capsule, which was placed adjacent to the source container (and therefore, at the same temperature) inside the silica glass tube. The tube was then inserted into the furnace in identical manner as the other experiments. The experiments containing an oxygen monitor were run for the same duration and quenched using the same technique as the monitor-absent experiments.

In recognition that gas exsolution is a time-dependent process, the duration of the experiments was varied from 12 to 96 hr in order to determine if there was a change in vapor-deposited assemblage. Likewise, in recognition of a thermal effect on gas/solid equilibria, the temperature of the source was changed. However, experimental technique limitations impeded our capability to explore this to any significant extent. The upper temperature limit of the experimental equipment used was 1200°C. Although the lower temperature limit (which is the S- and Cl-free low-pressure solidus temperature) could be readily attained, the rise in solidus temperature during degassing caused so much crystallization below 1150°C that the degassing melt was continuously changing composition. This added an uncontrolled compositional variable that we wished to avoid. For this reason, the difference in the hot spot temperature of successive experiments was only 50°C and likely uninformative.

4. Results

Each silica glass tube was carefully inspected before opening. A variety of experiments were deemed failures based on this inspection and discarded. In some cases, the $Au_{80}Pd_{20}$ capsule had corroded and the sample had contacted the glass tube. In other cases, the source magma had boiled over and escaped its capsule, pooling at the bottom of the silica glass, causing it to rupture, sometimes explosively. Any tube that showed cracks, even those for which rupture occurred during cooling (as observed in real time), was discarded. Every intact tube with a Cl- and S-bearing source showed rings of coatings visible to the naked eye (Figures 2 and 3). Coatings were not seen using the Cl- and S-free I(NVA) composition. The intact glass tubes remained sealed and stored at room temperature until they were to be analyzed. Table 2 lists the successful experiments.

Tubes from successful experiments were scored and split longitudinally, producing shards of the tube with crystals adhered to the inner concave surface. Once opened, the crystal coatings quickly darkened and turned yellow (Figure 4). This change was attributed to water absorption and/or oxidation and further indicated that the glass tube had remained sealed during and after the experiments. Unfortunately, this change complicated the analysis of the deposits because as they hydrated, the adhesion of the gold coating for scanning electron microscopy (SEM) observations was impaired, and hydration sometimes caused the deposits to slough off the inner wall of the tubes. Furthermore, euhedral vapor-deposited crystals commonly lost their morphology upon opening of the tubes and deliquesced into residues with no discernable crystal form. In attempt to preserve the crystals once the tubes were opened, they were stored in a vacuum desiccator until ready for SEM analysis. Even with this precaution, the loss of crystal form impeded the use of SEM imaging to identify some crystals through the characteristic morphological forms of their crystal system.

4.1. Source Material

The spent source material consisted of both crystals and glass, irrespective of use of glass or powdered reagent mixture as the initial source. Although the temperature at the hot spot likely remained above the liquidus temperature of the volatile-bearing initial sources, minerals crystallized from the silicate melts during degassing. Some of the crystals in the spent sources may reflect quench crystals arising from our inability to rapidly drop the temperature of such large experimental charges below the solidus (since the evacuated

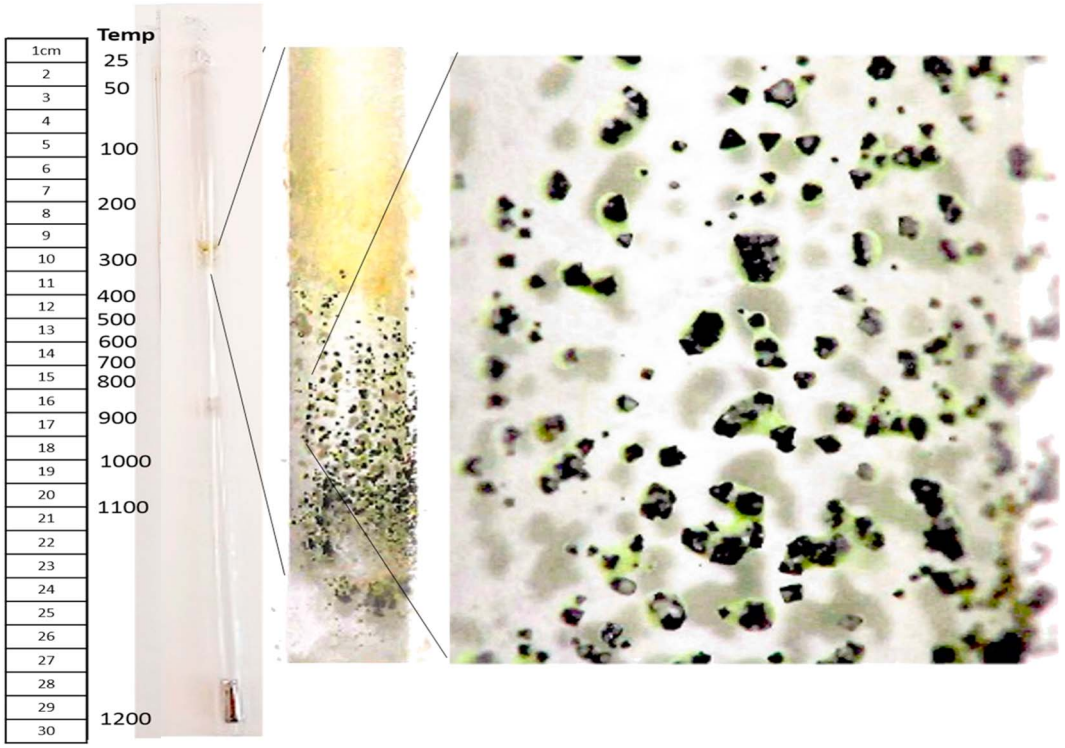

Figure 2. Silica glass tube containing I(Cl+S) glass source after cooling, with approximate temperature distribution in the furnace. Capsule containing the source is at bottom. Insets show enlargements of the region in the tube containing well-formed octahedra adhered to the tube by a fine-grained greenish-yellow precipitate. A ring of orange fine-grained material was formed just below ~300 °C.

tube acts like a vacuum bottle). However, some degree of isothermal crystallization is also expected simply due to loss of dissolved volatiles, specifically Cl (and H_2O) from the melt, and hence solidus temperature rise (e.g., Filiberto & Treiman, 2009). The spent source material was highly vesiculated, clearly indicating that boiling (vapor loss) had occurred and that we had indeed attained a high ratio of gas to silicate melt. The fine-grained, broadly disseminated crystals in the spent source made reliable electron microprobe analysis of the bulk composition of the spent source difficult.

Thermogravimetric analyses of I(Cl+S) glass source material were carried out in order to constrain how much mass was lost during degassing. This was done using a Netzsch STA 449C Jupiter Thermo-microbalance, where the sample was held in an alumina boat in an N_2 gas stream as temperature was ramped up slowly (10°/minute) to 1150°C. These measurements indicated that the source magma lost 8.3% of its weight during degassing. In addition, careful weighing of capsules loaded with I(Cl+S) reagent mix before and after degassing was made on a limited number of experiments where the capsule had not strongly adhered to the silica glass tube. The weight loss is within 1 wt% of the thermogravimetric analysis weight loss results for the glass source.

4.2. Vapor-Deposited Phases

4.2.1. Mineralogy

The crystals lining the upper portion of the tubes were small and strongly adhered to the inner walls, thus, making it difficult to mechanically remove them. Therefore, tubes were split open and broken. Glass shards were coated in gold for SEM and energy-dispersive spectroscopy (EDS) analysis to determine the morphology and chemistry of each mineral phase or coating present. These analyses were carried out using a LEO Gemini 1550 SEM with EDS capability at the Department of Materials Science at Stony Brook University. The identity of most vapor-deposited minerals was inferred from these observations.

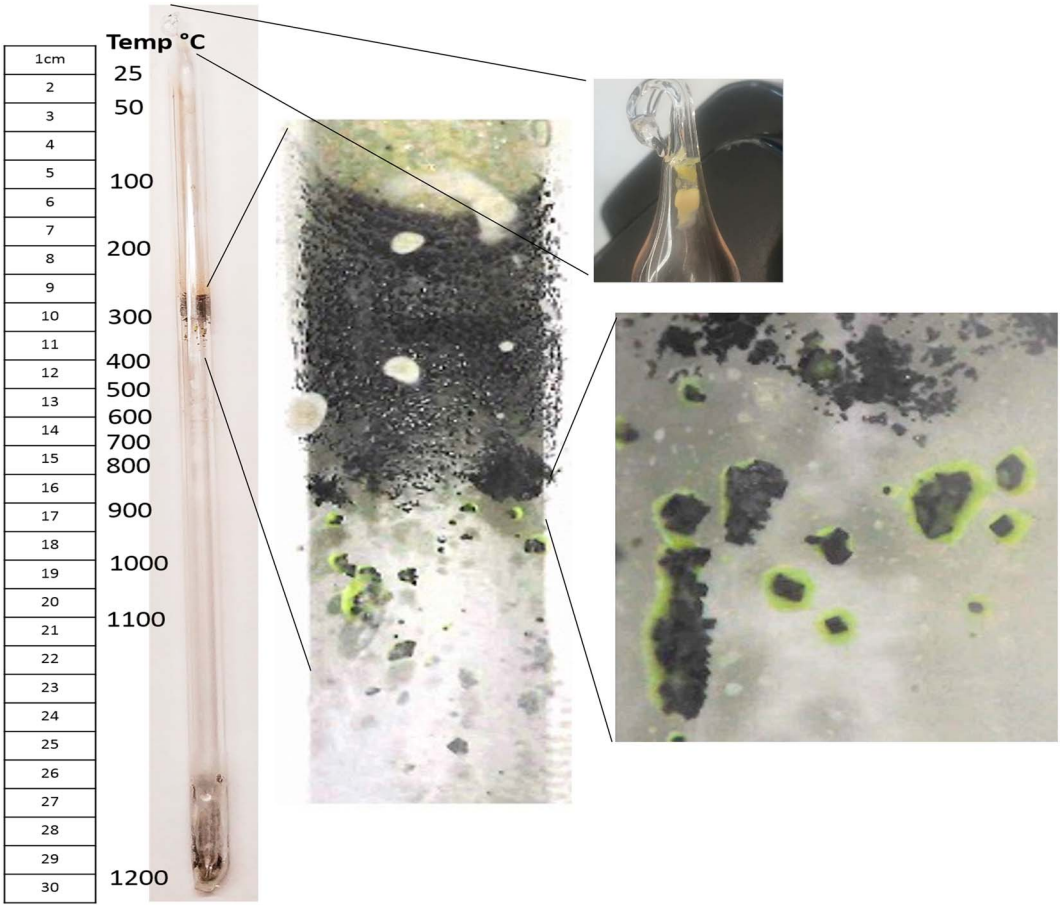

Figure 3. Silica glass tube containing I(Cl+HiS) glass source after cooling, with approximate temperature distribution in the furnace. Capsule containing the source is at bottom. Inset shows phases observed. Top image of right insets shows native S precipitate at top of the tube; the center and lower right insets show octahedra adhered to the glass wall by a greenish-yellow precipitate below a region of massive deposits of finer-grained dark material.

Table 2
Degassing Experiments, Sources, and Vapor-Deposited Phases Produced

Experiment	Source	*T* (°C)	Time (hours)	Halite	Sylvite	Molysite	Fe-sulfide	Silica	Fe_2O_3	S
A-22[a]	I(NVA) Glass	1150	12	No sublimates observed						
A-9	I(Cl+HiS) Glass	1200	12	✓	✓	✓	✓		✓	✓
A-13	I(Cl+HiS) Glass	1200	48	✓	✓	✓	✓	✓	✓	✓
A-60	I(Cl+HiS) Glass	1200	24	✓	✓	✓	✓		✓	✓
A-54	I(Cl+S) Glass	1200	24	✓	✓	✓			✓	✓
A-35	I(Cl+S) Glass	1200	12	✓	✓	✓		✓	✓	
A-36	I(Cl+S) Glass	1200	12	✓	✓	✓		✓	✓	
A-37	I(Cl+S) Glass	1200	12	✓	✓	✓			✓	
A-40	I(Cl+S) Glass	1200	12	sample used for ICP-OES						
A-24	I(Cl+S) Mix	1200	12	sample used for ICP-OES						
A-39	I(Cl+S) Glass	1150	24	✓	✓	✓		✓	✓	
A-30	I(Cl+S) Mix	1150	96	✓	✓	✓		✓	✓	
A-21[a]	I(Cl+S) Mix	1150	12	sample used for ICP-OES						

[a]Experiments containing an additional capsule with oxides used to monitor fO_2.
Abbreviation: ICP-OES, inductively coupled plasma optical emission spectrometry.

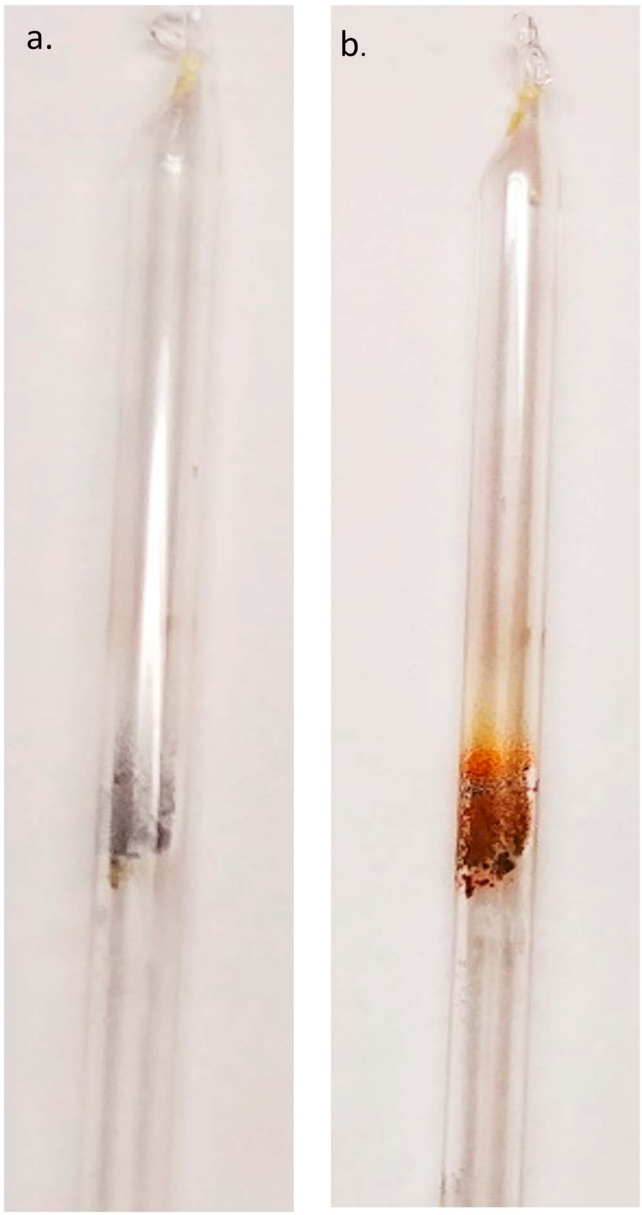

Figure 4. Silica glass tube containing I(Cl+HiS) glass source after experiment, (a) before and (b) after opening.

The crystal habit of grains that retained their form (as revealed by SEM) proved a useful phase indicator when combined with qualitative EDS analysis. Figures 5 and 6 show these forms and EDS spectra for both I(Cl+S) and I(Cl+HiS) sources. Halite (Figure 5a) was readily identified by both its chemistry and cubic habit. Sylvite (Figure 5b) is the inferred K- and Cl-bearing phase observed, based on EDS analyses as well as the likelihood that sylvite would be associated with halite. Iron chloride (Figure 5c) was found in all Cl-bearing experiments, identified using EDS only as it lacked a well-defined crystal form. EDS indicated the presence of an unknown silica phase in small rounded clusters (Figure 5d) in several experiments (Table 2); importantly, these were not found in the silica glass tube after the S- and Cl-free experiment and therefore were not simply related to the silica glass tube. Iron oxides crystallized from the vapor (Table 2) from both source compositions. They commonly formed octahedra, indicating a cubic crystal system and suggestive of magnetite or maghemite (Figure 5e). Native sulfur was deposited as bright yellow spherical blebs in the uppermost (coolest) location of the tubes (Figure 5f). In experiments using the I(Cl+HiS) source, two additional vapor-deposited minerals were observed. Pyrrhotite (or troilite) was identified through EDS and hexagonal/monoclinic morphology (Figure 6a). Pyrite was tentatively identified at the lowest temperatures of the (Cl+HiS) source experiments due to its cubic shape and higher S/Fe ratio (Figure 6b).

The identity of the Fe-oxide could not be determined directly by SEM. For this reason individual grains from the lower temperature region of the I(Cl+S) deposits (where the oxide octahedra were large and could be easily isolated) were removed from the glass shards, placed in paraben oil to prevent oxidation or hydration, and taken to the Advanced Photon Source of Argonne National Lab for Synchrotron X-Ray Diffraction (SXRD) analysis. Single-crystal XRD yielded unit cell parameters that most closely matched the maghemite (γ-hematite (a=8.337(7) Å, b=8.337(7) Å, c= 8.337(7) Å, and α=β=γ=90°) and α-hematite (a=b=5.0278(5) Å, c= 13.7368(15) Å, α=β=90°, and γ=120°) structures. The unit cell dimensions of maghemite indicate no titanium in the solid solution, that is, essentially end-member γ-Fe_2O_3.

The iron chlorides found were suggestive of molysite (ferric chloride) due to the highly deliquescent nature of this material and the formation of a yellow-colored liquid (brine) when exposed to moisture in the air (Figure 4). To verify this identification, confocal Raman spectroscopy was performed at the Vibrational Spectroscopy Lab at Stony Brook University on the high iron + chlorine coatings in sample A-9 and the spectrum compared to an analysis of dehydrated commercial-grade ferric chloride, $FeCl_3$. Analysis of both was carried out using a green laser with a wavelength of 514 nm. Figure 7 shows that similar features exist in both spectra at Raman shifts of 400, 500, and 670 cm^{-1}, supporting the conclusion that the iron chloride is molysite. The strong peak in the vapor-deposited material at ~200 cm^{-1} is a second phase coexisting with the molysite. Potential candidates of the second phase are sylvite and sulfur (for the high S composition), as these phases have peaks within the observed Raman shift range and both of these phases were already identified in this sample.

Coatings on the vapor-deposited minerals were also noted. These may have formed during cooling after removal of the tube from the furnace. Alternatively, particularly because of the droplet-like appearance of the regions in which they occur, some may have formed during dehydration of brine (formed either during cooling of the tube or when the deliquescent salts were exposed to air after opening the tubes) upon exposure to the SEM vacuum. As seen in Figure 5g, there is permissive evidence that iron oxychloride formed in this way.

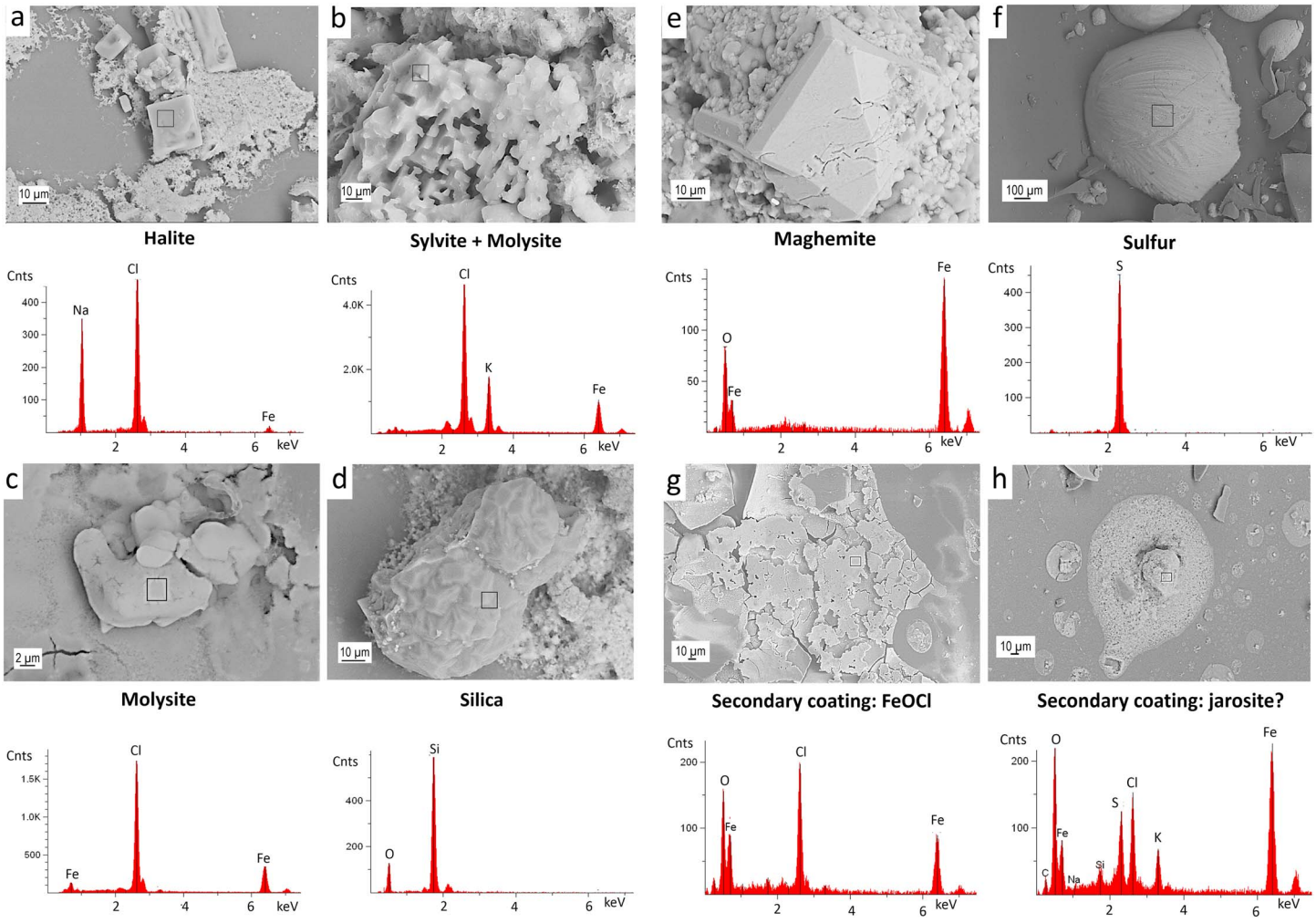

Figure 5. Scanning electron microscopy images, energy-dispersive spectroscopy spectra, and inferred identity of vapor-deposited minerals. (a) Halite, (b) sylvite, (c) molysite, and (d) silica were found in vapor deposits from the I(Cl+S) source in the temperature zone 800-300 °C and from the I(Cl+HiS) source in the temperature zone 700-300 °C. (e) Iron oxide is maghemite that may have originally been magnetite and joins the assemblage from the I(Cl+S) source at 500 °C and from the I(Cl+HiS) source at 700 °C and persists to 300 °C for both sources. (f) Sulfur is produced from both sources once the temperature is <100 °C. After cooling the tubes, coatings of FeOCl (g) and possibly halogen-bearing jarosite (h) were observed on the primary vapor-deposited minerals and on the inner walls of the glass tube from both sources.

Table 2 summarizes the vapor-deposited phases positively identified for each experiment. As only two source compositions were used, additional experiments tested the replicability of the technique. Importantly, due to the large areal extent of the interior of the long tubes and the small SEM footprint, only the presence of a phase directly analyzed by SEM is definitive as absence may simply be a result of a phase being overlooked due to small grain size or discontinuous distribution within the tube. Experiments A-35, A-36, and A-37 exemplify this. They show that the vapor-deposited assemblage should include maghemite and silica even though analysis of two of the three tubes showed only one of these two phases. Because of the strong possibility that a phase could be overlooked in the tube, the identification of a new phase in replicate experiments, but for longer duration of the degassing, does not mean that the phase was not present after the shorter duration degassing. This may be exemplified by the presence of silica in the assemblage of experiment A-13, but not in A-9; it may simply have been overlooked in A-9 perhaps because of smaller cluster size. The apparent lack of hematite in the long-duration experiment A-30 using a powder source, but its identification in the shorter duration run using glass source (A-39), may similarly be caused by oversight. Within the small temperature difference investigated here using the glass source no temperature-induced difference in vapor-deposited assemblages was noted.

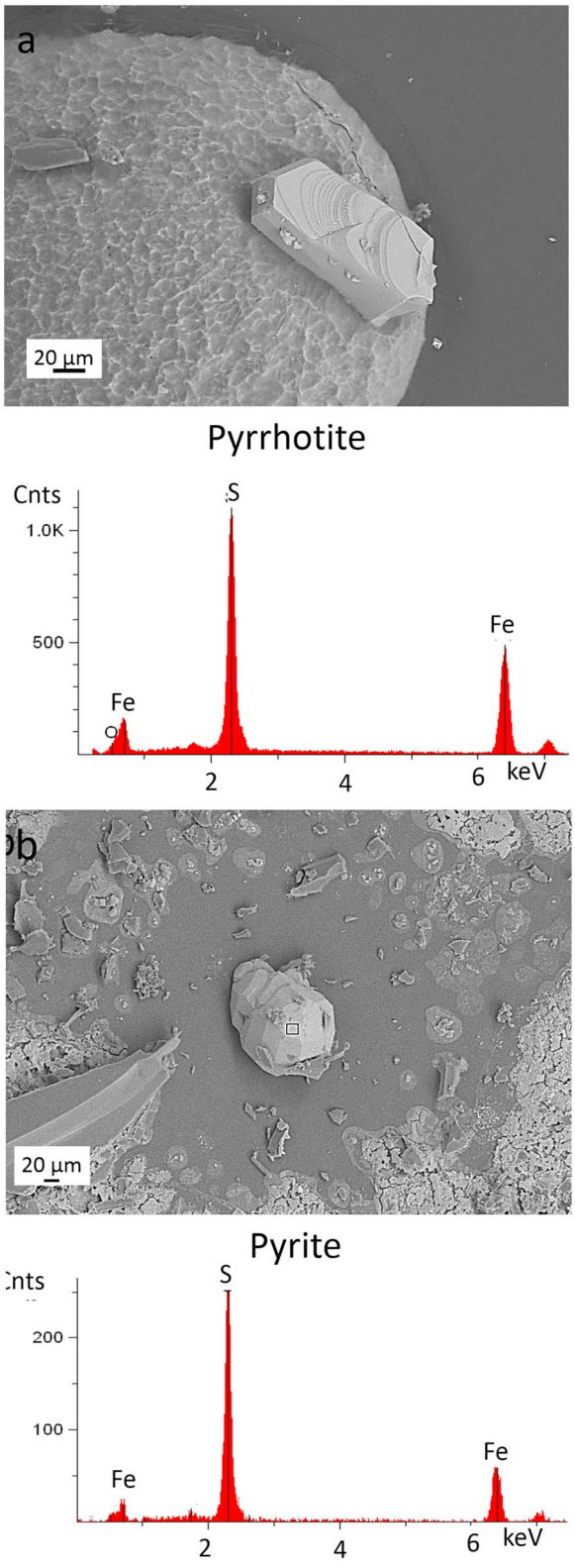

Figure 6. Scanning electron microscopy images, energy-dispersive spectroscopy spectra, and inferred identity of vapor-deposited minerals unique to the I(Cl+HiS) source. (a) Pyrrhotite (or troilite) which joins the halite + molysite + sylvite + maghemite assemblage at 500 °C and persists to 300 °C. At 300 °C, (b) pyrite replaces pyrrhotite as the primary sulfide.

4.2.2. Composition of Bulk Vapor-Deposited Material

For experiments A-21, A-24, and A-40 of Table 2 using the I(Cl+S) source, the identities and relative abundances of cations within the upper part of the tube that contained most of the vapor-deposited material were determined by inductively coupled plasma optical emission spectrometry (ICP-OES) analysis. After each of these experiments, the upper portion of the tube containing the visible deposits was first weighed, then fully submerged in a 3M nitric acid solution and left to soak at room temperature for several days. After all visible solids were dissolved from the interior of the tubes, the tubes were removed from the solution, dried, and reweighed. The mass of total dissolved vapor-deposited solids in each partial tube was obtained by the weight of the tube before and after dissolution. The total concentration (by weight) of the dissolved deposits in the acid solution is the weight of total dissolved solids/amount of acid and is listed in Table 3 as total solid concentration. Importantly, if hydration (or oxidation) of any mineral phase (e.g., hydration of molysite to $FeCl_3.6H_2O$) took place prior to weighing of the glass tube (before acid dissolution), the weight of total dissolved solids would be artificially elevated. Therefore, the partial tubes were weighed as soon as they were removed from the drying oven.

The nitric acid solutions containing dissolved vapor-deposited material were analyzed by ICP-OES for all of the cations present in the source material (Table 1); however, only Na, K, and Fe had concentrations above 1 ppm (mg/L). Note that this analysis did not include Si because it would not be possible to distinguish Si dissolved from the silica glass tubes from dissolved vapor-deposited Si. Table 3 summarizes compositional data for the solute from the dissolution. Iron is the most abundant cation in the deposits with lesser amounts of Na and K. The concentration of each of the other cations analyzed is less than 1 ppm, with many on the order of tens of ppb, consistent with their absence in the mineral phases identified by SEM. Mass balance for the cations listed in Table 3 based on the total solids concentration can be met by a combination of primary halite, sylvite, molysite, Fe_2O_3, and secondary ferric chloride hexahydrate. However, because of nonuniqueness, the relative abundance of each of the Fe-bearing minerals is uncertain. The differences between the analysis of A-21 and A-24 indicate the relative uncertainty, as the same source I(Cl+S) mix was used. The difference in total concentration of solids for the glass source rather than the mix is most likely due to the lower amount of glass source used in experiment A-40 compared to the amount of mix in experiments A-21 and A-24.

The ICP-OES results indicate that alkali complexes preferentially degassed relative to Fe complexes as suggested by the lower Fe/total alkalis (molar) ratio in the vapor deposits (Table 3) relative to that of the starting material (e.g., 3.1-3.5). This reduction in Fe/total alkalis (molar) was greater for the glass source than the mix source suggesting that Fe may have been more tightly bound in the glass source. Perhaps with longer experimental run times, however, these different source structural states would have yielded the same bulk cation abundance of the vapor-deposited material. Nonetheless, both source types produced the same vapor-deposited mineralogy. This suggests that variations in the degassing path for Cl and S-bearing magmas may produce similar vapor-deposited minerals.

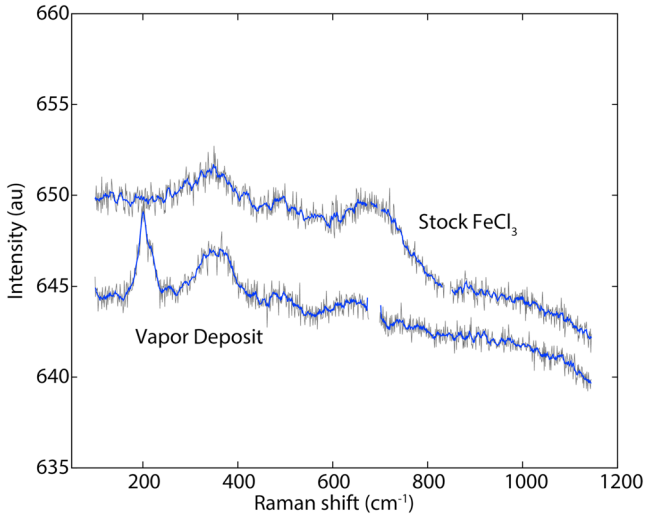

Figure 7. Comparison of Raman spectra from dehydrated laboratory-grade ferric chloride and vapor deposited material from experiment A-9 containing an iron-chlorine compound. Features at 400, 500, and 670 cm^{-1} suggest that the sublimate contains ferric chloride (molysite). The strong peak in the vapor deposit is a second crystalline phase, likely deposited at the same time as the molysite. The gap in the spectrum at ~700 cm^{-1} corresponds to a cosmic ray detected during the analysis and deleted from the data. Intensity is shown in arbitrary units. Raw data are shown in gray; blue lines represent data smoothed with a seven-channel boxcar filter.

4.3. Oxygen Fugacity of the Source

The oxygen monitor assemblages were recovered when the tubes were opened. XRD analysis of the monitor in the Cl- and S-free experiment (Experiment A-22 I(NVA) at 1150 °C) coupled with the calibration of the variation of 2Θ with oxide composition of Lindsley (1976) showed a slight shift to a more oxidized compositional pair (Table 4 and Figure 8) from $Usp_{48}Mt_{52}$ and $Il_{72}Hm_{28}$ to $Usp_{44}Mt_{56}$ and $Il_{70}Hm_{30}$ and an increase in Hm solid solution abundance relative to spinel (as seen by the intersection of the tieline and "redox" line in Figure 8), consistent with oxidation. This small change in composition of the oxide pair yields a change in oxygen fugacity within the uncertainty of QUIlF calculations and indicative of NNO+0.6($\pm$0.1) log units. The fact that the X-ray pattern showed a clear, albeit small, change from the original monitor suggests that the monitor acted as a redox probe, not as a buffer, and that the redox state of the source was slightly higher than NNO. If the oxides attained equilibrium within the run duration, then the oxygen fugacity is constrained to have been NNO+0.6. Based on the experimental durations of Webster and Bright (1961) for oxides far from equilibrium, it is likely that the oxide pair in our experiments had sufficient time to equilibrate. Since water was the only major dissolved volatile in the I(NVA) source, the absence of a major shift in composition of the monitor verified that loss of water alone by degassing did not affect the redox state at the hot spot (Waters & Lange, 2016).

Based on the XRD spectrum of the monitor in the A-21 experiment (which used the I(Cl+S) source), the oxides showed significantly more oxidation than those in the Cl- and S-free composition, shifting from the assemblage $Usp_{48}Mt_{52}$ and $Ilm_{72}Hm_{28}$ to $Usp_{29}Mt_{56}$ and $Ilm_{60}Hm_{40}$ after the degassing. When computed through QUIlF however, these oxide compositions do not represent an equilibrium pair at the temperature of the source; instead, they indicate a temperature of over 150 °C lower than the actual temperature. If the Ilm_{ss} composition is correct, the coexisting Usp_{ss} should have been $Usp_{40}Mt_{60}$ (Figure 8). This would suggest that the ulvöspinel solid solution was preferentially oxidized relative to the ilmenite solid solution upon exposure to the magmatic gas. If the Ilm_{ss} composition is incorrect, the computed Ilm_{ss} ($Ilm_{48}Hm_{52}$) would not preserve the bulk Fe/Ti ratio of the initial monitor and would suggest that Fe was transported to the oxides by the gas. Either situation suggests that the gas may react with the oxides, making a two-oxide monitor unreliable at best, and that this interaction has the potential to change the gas chemistry. Therefore, additional experiments were not run with an oxygen monitor.

Table 3
Bulk Cation Abundance of Vapor-Deposited Phases From ICP-OES

Source		I(Cl+S) mix		I(Cl+S) glass		I(Cl+S) mix	
Experiment		A-21		A-40		A-24	
	λ[a]		1σ[b]		1σ		1σ
Fe (ppm)	259.94	48.82[b]	0.27	32.57	0.06	51.59	0.23
K (ppm)	766.49	3.88	0.04	3.42	0.01	4.31	0.03
Na (ppm)	589.59	10.07	0.10	2.21	0.01	9.87	0.02
Total solids[c] (mg/L)		162.8		63.5		157.1	
Fe/(Na+K)[d]		1.63		1.09		1.72	

[a]Emission line wavelength (nm). [b]Based on triplicate analyses. [c]mg_{solute}/L_{acid} based on weight of tube before and after dissolution of vapor deposits in nitric acid and acid removal. [d]Cation molar ratio.
Abbreviation: ICP-OES, inductively coupled plasma optical emission spectrometry.

5. Discussion

The results of the degassing experiments of the Cl- and S- bearing source compared with the Cl- and S-free source underscore the importance of Cl and S in magmas for the formation of vapor-deposited phases. The experimental setup yielded sufficient quantity of deposited material for analysis; furthermore, the replicate experiments showed that reproducible results were readily obtained. The experiments produced deposits generally consistent with the vapor-deposited minerals collected at the Erta Ale vent (e.g., Zelenski et al., 2013). However, just as for terrestrial fumarolic gas sampling in glass tubes, correlating a precise temperature with a specific assemblage is not straightforward because of the superposition of cooler phases during cooling of the tubes. For the experiments, cooling upon removal of the glass tube from the furnace after the experiment may have caused oxidation in addition to secondary reactions; opening the tube for analysis may have induced hydration.

Table 4
Powder X-ray Diffraction Data for Two-Oxide Monitors and Inferred Compositions of the Oxides

Co-existing oxides of unreacted monitor				Co-existing oxides Experiment A-22 I(NVA) source				Co-existing oxides Experiment A-21 I(Cl+S) source			
Ilmenite-Hematite$_{ss}$		Ulvospinel-Magnetite$_{ss}$		Ilmenite-Hematite$_{ss}$		Ulvospinel-Magnetite$_{ss}$		Ilmenite-Hematite$_{ss}$		Ulvospinel-Magnetite$_{ss}$	
2Θ	Ilm (mol%)	2Θ	Ulv (mol%)	2Θ	Ilm (mol%)	2Θ	Ulv (mol%)	2Θ	Ilm (mol%)	2Θ	Ulv (mol%)
48.97	72.5	52.98	48	49.01	69	53.03	43.5	49.07	61.5	53.19	29
53.42	71	56.47	47.5	53.44	69	56.53	42.5	53.57	58	56.68	28
61.84	70	62	49.5	61.85	70	62.03	47	61.96	59	62.29	28
63.48	72.5	70.33	47	63.47	74	70.37	45	63.57	62	73.58	31
70.79	72	73.29	49	70.87	67.5	73.37	44	70.06	57.5		
		74.29	48			74.36	44.5				21.3
Avg	72		48	Avg.	70		44	Avg.	60	Avg.	29

In the experiments with the I(Cl+S) source, Fe/Na/K chlorides are found throughout the temperature region ~800-300 °C, with evidence of silica deposits in this region as well (where the temperature regions mentioned reflect the original temperatures of the experiment before removal from the furnace and cooling of the tube). Within the temperature regime 500-300°C, abundant maghemite appears as individual grains embedded in a matrix of chlorides (molysite+halite+sylvite). However, the greenish color of the chloride that adhered the maghemite to the glass tube prior to opening the tube and exposure to air hints that the primary iron chloride precipitated by the gas may have actually been lawrencite ($FeCl_2$) and that the molysite was secondary to oxidation of lawrencite. The maghemite is likely also secondary, having perhaps formed from oxidation of primary magnetite during cooling of the tube (e.g., Jubb & Allen, 2010; Salazar

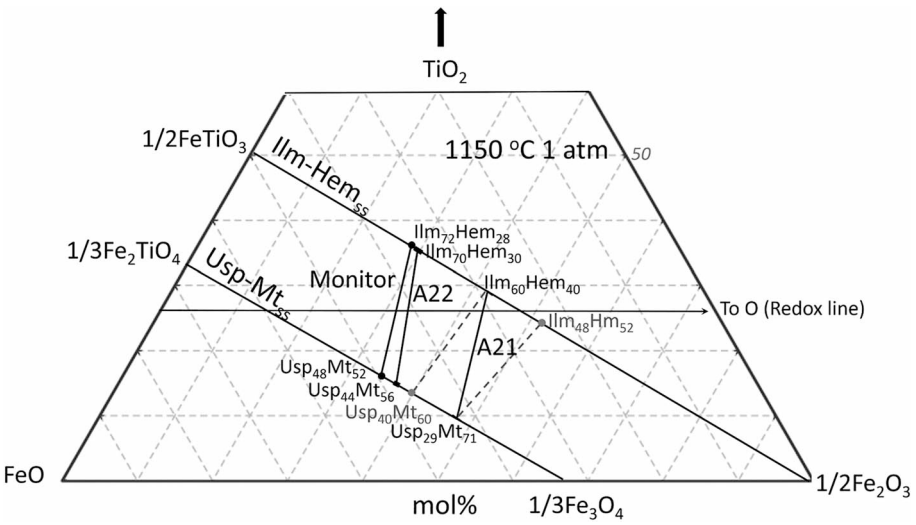

Figure 8. Compositions of co-existing ilmenite-hematite (Ilm-Hm$_{ss}$) and ülvospinel-magnetite (Usp-Mgt$_{ss}$) solid solutions of the initial monitor and of the monitor after heating with the I(NVA) source, experiment A-22 (A22), and the I(Cl+S) source, experiment A-21 (A21), indicated by solid tielines in a subsystem of the system FeO-Fe_2O_3-TiO_2. The Ilm-Hm and Uspt-Mt solid solution lines were computed from QUIlF (Andersen et al., 1993) for 1150 °C and 1 atm. The oxide compositions (see Table 4) are based on cell parameters and the variation of cell dimensions with changing composition of the solid solutions from powder X-ray diffraction and the assignments of Lindsley (1976). The redox line shows the direction of oxidation for the Fe/Ti ratio of the oxide mixture. Note that the intersection of the monitor tieline with the redox line shows the 1:1 ratio of Ilm-Hm$_{ss}$ and Usp-Mgt$_{ss}$ loaded for the initial monitor. The composition of the monitor after the A22 experiment shows evidence for oxidation not only in the shift of oxides composition but also in the slight increase in modal abundance of IlmHm$_{ss}$. The monitor oxides after the A21 experiment shows strong oxidation, and produced a disequilibrium pair. The dashed gray tielines indicate the computed equilibrium pair for A21 assuming, in turn, that one of the oxides in A21 had reached equilibrium during the experiment.

et al., 2011). Below 300°C, few deposits are visible other than a ring of orange material on the glass that may have been hydrated ferric chloride (perhaps ferric chloride hexahydrate). Native sulfur is found at the coolest end of the tube. All phases within the region of 700-500°C appeared to have secondary coatings that may have been produced during cooling of the tubes, by reaction among vapor deposited minerals or by gas/mineral interaction, with iron oxychloride as the most significant example. Hematite was noted with maghemite during analysis of a single octahedron; this may have formed by oxidation upon cooling of the tube after the experiments.

For the sulfur-rich source, iron oxides are visibly precipitated with chlorides at ~700°C, along with silica deposits. At ~500°C is a region with the assemblage sylvite+halite+ molysite+pyrrhotite+maghemite, which, before cooling of the tube, may have been the primary assemblage sylvite+halite+lawrencite +pyrrhotite+magnetite. Below about 400°C iron oxides are no longer observed. Sulfides, specifically pyrite, persist to as low as 300°C, at which point chlorides are no longer found. At the lowest temperatures, <100 °C, native sulfur "droplets" are adhered to the top of the tube.

The experiments do not provide access to direct information on the gaseous species during the experiments, but some inferences can be made based on the assemblages. With 0.4 wt.% water in the starting glass, there was undoubtedly some H-bearing gaseous species present in the vapor phase. S-species in the vapor would be dominantly SO_2 at the pressure of the experiments (~1 bar), with significant S_2 and minor H_2S (Gaillard & Scaillet, 2009). Some of the Cl was likely transported as HCl. However, as it is generally accepted that the vapor species of salts and oxides in high temperature gases are associated units (Krauskopf, 1964; Renggli et al., 2017), additional metal chloride gaseous species were likely also present. Although we cannot definitively correlate the deposited minerals with an equivalent charge-neutral associated vapor species (Renggli et al., 2017), the fast, high-temperature deposition in the silica glass tube suggests a simple process of sublimation (Yudovskaya et al., 2008). In this case, the Fe content of the net composition of the vapor-deposited material would be primarily due to the transport of Fe as iron chloride, iron oxide, and iron sulfide gaseous species, as concluded by Renggli et al. (2017). The high Fe content of the net vapor deposit composition is likely correlated to the high Cl content of the melt, as Fe-chloride complexes can partition even more strongly than NaCl and KCl into exsolved fluid, liquid, or gas (Pokrovski et al., 2013).

5.1. Redox Conditions of the Gas in the Tube

Assessing the distribution of oxygen in the tube is important as oxygen plays a central role in dictating the redox state of the gaseous species. It is commonly assumed that in experiments utilizing short evacuated silica glass ampoules (i.e., in a small temperature gradient), that the oxygen fugacity throughout the tube in "nominally volatile-free" systems equals that of the sample at the hot spot, even without an additional oxygen buffer. This conclusion still holds for long evacuated tubes in a strong thermal gradient but only as long as O_2 is the sole gaseous species. This can be seen by the generalized expression for diffusion of a chemical species in the absence of external forces over a thermal gradient:

$$\mathbf{J}_\mathrm{i} = -\mathrm{D_i C}\mathbf{d}_\mathrm{i} - \left(\mathrm{D_i}^{(\mathrm{T})}/\mathrm{M_i}\right)\ \nabla \mathrm{lnT}$$

(equation 14.6-1 of Deen, 2013) where $\mathbf{J}_\mathrm{i}$ is the diffusive flux of chemical species i, $\mathrm{D_i}$ is the diffusion coefficient of species i, C is the overall concentration of the phase at a point in space, $D_i^{(T)}$ is the Soret thermal diffusion coefficient, M_i is the molar mass of species i, and T is the temperature.

$$\mathrm{C}\mathbf{d}_\mathrm{i} = (1/\mathrm{RT})\left(\mathrm{C_i}\ \nabla_{\mathrm{T,P}}\ \mu_\mathrm{i} + (\mathrm{C_i V_i} - \omega_\mathrm{i})\ \nabla \mathrm{P}\right),$$

that is, $\mathrm{C}\mathbf{d}_\mathrm{i}$ is the sum of diffusion from the isothermal, isobaric chemical potential gradient and isothermal diffusion from molar volume differences in a pressure gradient, where C_i is the concentration of species i; $\nabla_{T,P}\mu_i$ is the isothermal, isobaric gradient in chemical potential of gaseous species i; V_i is the partial molar volume of species i; ω_i is the volume fraction of species i in the phase; and ∇P is the pressure gradient between two specified points.

If oxygen is the only gaseous species, the Soret Thermal Diffusion coefficient, $D_i^{(T)}$, is zero since the Soret effect (thermal gradient-driven diffusion) is not observed in pure phases (Platten, 2006). Additionally, the $(C_iV_i\text{-}\omega_i)\nabla P$ term is zero in a pure gas, since the molar volume of i is the inverse of the concentration of

the species i and ω_i is 1. Therefore, even in a temperature gradient, the diffusion of species i reduces to the Teorell equation (Gorban et al., 2011):

$$\mathbf{J}_\mathrm{i} = -u_i \ \nabla_{T,P}\mu_i$$

where u_i is the mobility of species i. At steady state in the tube, in the absence of a reaction and with no convective motion,

$$\mathbf{J}_\mathrm{i} = 0 = -\mathrm{u}_\mathrm{i} \ \nabla_{\mathrm{T,P}}\mu_\mathrm{i}$$

where u_i is approximately constant. Because of this, oxygen in the silica glass tube will diffuse until the chemical potential of oxygen is the same throughout the tube (that is, the chemical potential gradient must be zero) along the thermal gradient. As long as the fugacity coefficient is approximately 1 (a very reasonable assumption for a dilute pure gas phase at moderate temperature), oxygen must diffuse throughout the entire tube until the pressure is equalized at all points regardless of temperature. Combined with the boundary condition that the fugacity of oxygen at the position of the source is that of ~NNO at 1150°C, at steady state, diffusion will occur until the fugacity of oxygen throughout the entire tube is that of the source at the hot spot. The requirement that the oxygen fugacity be the same throughout the tube in this case precludes a change in oxygen fugacity along an oxygen buffer curve in the cooler portion of the tube. Because of the stronger oxidizing effect of a given oxygen fugacity at lower temperatures, constant oxygen fugacity would produce assemblages that were more oxidized at higher levels in the tube. The condition of constant oxygen fugacity throughout the tube is not retained however, in a multicomponent gaseous mixture where O_2 is a minor constituent. But it can be considered as providing the upper limit of oxygen fugacity in the system.

For a multicomponent vapor, the two components of the overall diffusion equation which we set to zero—one for thermal-driven diffusion and one for molar volume differences-driven diffusion—would be nonzero. If the quantity of other gases were small compared to the quantity of O_2, we could neglect the thermal driven diffusion, and as a result, no pressure gradient would form, and we would recover our original result. But for the multicomponent gases produced in these experiments (where O_2 is a minor constituent), thermal diffusion (known as the Soret effect in liquids) becomes an important player. This is a well-recognized phenomenon, which causes concentration gradients to develop in an originally homogeneous gas mixture placed in a strong temperature gradient (e.g., Bogatyrev et al., 2014; Chapman & Cowling, 1953; Chapman & Dootson, 1917; Gillespie, 1939). This compositional gradient can exist in steady state due to a balance between ordinary diffusion (which tends toward homogenization) and thermal diffusion (which induces a separation of species; e.g., Deen, 2013). While no pressure gradient would develop in the tube, the species with larger mass will be preferentially concentrated at the cold end (e.g., Chapman & Dootson, 1917; Deen, 2013). Therefore, the concentration of oxygen is predicted to be lower at the cold end of the tube relative to the concentrations of gaseous species such as SO_2 and neutral salt complexes such as $FeCl_{3(g)}$.

Since thermal diffusion coefficients are difficult to obtain due to their temperature and compositional dependence, assigning numerical values to the oxygen gradient in the tube is not possible, yet the assemblages observed may produce some qualitative indication of oxygen fugacity distribution in the tube. The oxygen fugacity set at the hot spot based on the results of the I(NVA) oxygen monitor experiment was NNO+0.6±0.1. Figure 9 provides a reconstruction of the oxygen fugacity along the tube based on observed phase assemblages and the assumptions that (i) the sulfides and oxides are primary vapor-deposited minerals and their position in the tube reflects the thermal gradient in the experiments; (2) maghemite formed by oxidation of magnetite, so its presence indicates magnetite as the vapor-deposited phase; (3) the hematite associated with maghemite in I(Cl+S) is secondary; that is, it formed during cooling after removal of the tube from the furnace; and (4) the regions of the tubes removed for analysis adequately reflect the temperatures regime noted. As shown in Figure 9, for both sources, the presence of magnetite restricts the oxygen fugacity to the region between the HM and WM buffer curves over much of the temperature space. Thus, there is a definite decrease in oxygen fugacity with increasing distance from the hot spot (decreasing temperature). Because no buffer was present in these experiments, the lower fO_2 at lower temperatures in the tube can likely be ascribed to the thermodiffusion of gaseous species discussed above.

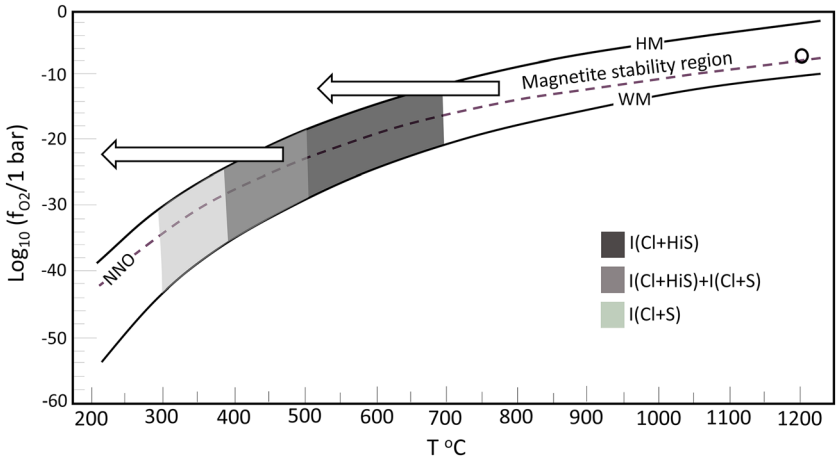

Figure 9. Constraints on the variation of the oxygen activity (fugacity/1 bar) with temperature along the thermal gradient in the silica glass tubes during the experiments based on the presence of vapor-deposited magnetite (assuming primary precipitation of magnetite before later conversion to maghemite upon removal of the tube and cooling). Open circle is the initial source at 1200 °C. The legend indicates the sources used in each region. HM: hematite-magnetite buffer; WM: wustite-magnetite buffer; NNO: nickel-nickel oxide buffer all computed using the Robie et al. (1979) database. The decrease in oxygen fugacity with decreasing temperature along the thermal gradient in the tube is likely due to Soret diffusion in the tube in these buffer-free experiments. Arrows indicate the oxidation that would accompany cooling at any one location in the tube upon removal of the tube from the furnace. This would change for example, magnetite to maghemite and finally to hematite.

5.2. Implications for Martian Fines

Magmatic vapor escaping from gas bubble-charged shallow magmas may have contributed a significant amount of Fe, S, and Cl to the Martian surface through vapor-deposition of minerals during the late stages of Martian magmatism when the gas ascending from a deep plumbing system was OH-poor and S- and Cl-rich. Such deposits would not have been restricted to large gas vents but could have been distributed across the surface of lava flows during passive gas loss. This process would not transport significant amounts of Ca, Mg, (or Al) from the magma and hence would preclude the direct deposition of Ca- or Mg-sulfates. Although direct vapor deposition of Ca- and Mg-sulfates seems unlikely based on these experiments, such sulfates could form during acid alteration of the surface via gas/rock interaction (e.g., Chouinard et al., 2005; King et al., 2018; Stoffregen, 1987).

Passive degassing of a bubble-charged lava flow involves strong thermal gradients above the lava surface and a change in the thermal profile with time as cooling of the surface of the flow occurs. In this case, a clear spatial variation in type of vapor-deposited material would not be expected. Instead, there should be mixed regions of high and low temperature vapor-deposited assemblages reflecting cooling of the gas above the flow. The mineral phases of the intermingled assemblage could react upon dropping temperature (as the thermal gradient above the lava flow collapsed) and form a set of secondary minerals that obscure at least some of the primary assemblages. These secondary minerals could have been disproportionately represented in the Martian fines. Such reaction could occur with no free surface water. Changes in relative humidity as observed by MSL (Savijärvi et al., 2015) can lead to deliquescence and subsequent efflorescence of some salts (e.g., Gough et al., 2014, 2016; Nuding et al., 2014), potentially allowing deliquescent phases to incorporate other elements from soluble salts as they become brines and then re-solidify (Sklute et al., 2018).

The absence of magnetite but plentiful octahedra of the metastable phase maghemite suggests efficient conversion of magnetite to maghemite as a consequence of the formation of a more oxidized assemblage upon cooling of the tube after it was removed from the furnace. The possibility of maghemite being present at the surface of Mars is evidenced by analysis of magnetic dust in situ (Bertelsen et al., 2004). Since the magnetic properties of Martian dust and soil are presumed to be dictated, as on Earth, by magnetite and maghemite (Banin et al., 1993; Madsen et al., 1999; Morris et al., 2000, 2001), the production of maghemite by vapor deposition on the surface of cooling lava flows provides an important alternative production mechanism to that of the thermal conversion of lepidocrocite via meteoritic impact (Banin et al., 1993; Morris et al.,

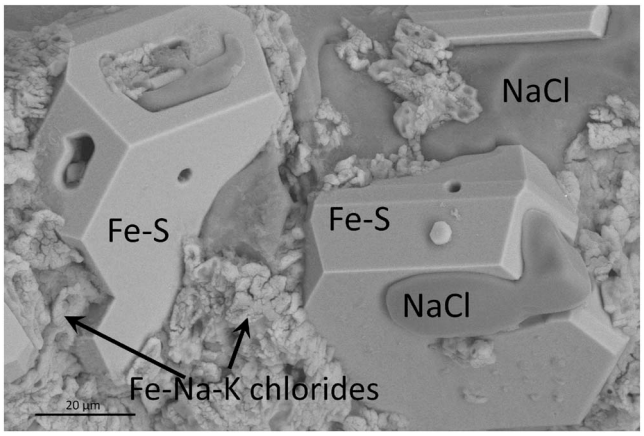

Figure 10. Backscattered electron image of coexisting vapor-deposited phases produced using the I(Cl+HiS) source.

1998) or its formation as a transient phase in the transformation of ferrihydrite to hematite in the presence of phosphate or other ligands capable of ligand exchange with Fe-OH surface groups (Barron & Torrent, 2002; Cumplido et al., 2000; Torrent & Barrón, 2000).

The coexistence of molysite and hematite (and maghemite) in the vapor-deposited assemblages allows for the formation of iron oxychloride (FeOCl) by the reaction $FeCl_3 + Fe_2O_3 \rightarrow 3FeOCl$ at ~350°C (Dai et al., 2003; Halbert et al., 1980; Yang et al., 2013). This phase may be reflected in the EDS spectrum of Figure 5g and present in the fine-grained coatings. Iron oxychloride is a Fenton-like catalyst, which according to Yang et al. (2013) exhibits unusual efficiency for yielding OH radical by H_2O_2 decomposition and exceptional performance in the degradation of persistent organic compounds (e.g., from carbonaceous chondrite impactors or other organic sources). This has important implications for Mars in that it suggests if iron oxychloride produced in the cooling gas column above Martian lava flows couples with a photochemically produced atmospheric oxidant such as H_2O_2 (Atreya et al., 2006), it would contribute to destruction of organics on the Martian surface. In fact, a lower than expected organic yield has been noted by Zent and McKay (1994) based on the Viking Biology Experiments and Ming et al. (2014) in their discussion of the analysis of the mudstone at Yellowknife Bay, Gale crater.

There are various routes to destruction of FeOCl that could inhibit its identification in Martian fines. Iron oxychloride readily picks up atmospheric moisture and can produce akaganéite (FeO (OH,Cl); Argo, 1981), a phase seen in the mudstone at Yellowknife Bay (e.g., Vaniman et al., 2014) and at Vera Rubin Ridge (Morris et al., 2019), Gale Crater, or it can produce Fe $(OH)_2Cl$, even at temperatures below 100°C. Upon heating, Fe $(OH)_2Cl$ can lose some HCl and revert to FeO (OH,Cl), or, if all HCl is lost, form β-FeOOH (Kanungo & Mishra, 1997). Perhaps Fe $(OH)_2Cl$ contributed to the HCl release detected by the Sample Analysis at Mars (SAM) instrument on board the MSL Curiosity rover in Gale Crater (Hogancamp et al., 2018). Under even more humid conditions, FeOCl (or molysite directly) may have formed ferric chloride hexahydrate as the magmatic gas cooled below 220–250°C (Zhang et al., 2017), which was then deposited into the fines. Dehydration of any ferric chloride hexahydrate during heating and analysis would have contributed to the reported water budget yielded by heating samples from Rocknest fines and the mudstone of the Yellowknife Bay Formation. Importantly, chlorides may also have produced perchlorates on the Martian surface by interaction with atmospheric oxidants, irradiation of the Martian surface by either UV (Carrier & Kounaves, 2015; Schuttlefield et al., 2011) or cosmic rays (Wilson et al., 2016), or through electrostatic discharge during dust storms (Wang et al. 2019 and references cited within). This last process may also produce a significant amount of amorphous material. FeOCl or Fe-perchlorate could have contributed to the O2 and Cl observed through Curiosity's Sample Analysis at Mars instrument suite to been given off during heating of the Rocknest aeolian deposit (Leshin et al., 2013).

The spatial association of halite, molysite, and pyrrhotite in the vapor-deposited material (Figure 10) suggests that in the presence of small amounts of water and upon oxidation of the pyrrhotite, all of the ingredients for making fine-grained jarosite would be available. Dutrizac (2008) noted that jarosite is readily precipitated upon dissolution of KCl (and NaCl) and molysite, provided that an independent source of sulfate is available. His experiments at 140°C indicated that low sulfate concentrations resulted in the precipitation of hematite-jarosite mixtures; higher sulfate concentrations result in the formation of only potassium jarosite. This jarosite formation could occur as the surface of the lava flows continued to cool below 200°C. By this temperature, as seen in the I(Cl+HiS) experiments, pyrite rather than pyrrhotite would be stable and oxidation of pyrite could be an important step in the formation of jarosite (Zolotov & Shock, 2005). McCubbin et al. (2009), however, noted the presence of secondary jarosite and hematite surrounding pyrrhotite in a melt inclusion in pyroxene from the Miller Range 03346 meteorite, suggesting that the conversion of pyrrhotite to pyrite may not be a necessary first step. Since liquid water is not necessary to form the jarosite according to the calculations of Navrotsky et al. (2005), it is possible that the fugacity of water was sufficiently high in the magmatic gases by this stage and enhanced by relative humidity of the Martian atmosphere that this process could have occurred in the absence of liquid water. The presence of halogens in

the jarosite may reduce the relative humidity needed to produce halogen-free jarosite. Such halogen-bearing jarosite may be represented in some of the coatings seen in these experiments (Figure 5h). The formation of halogen-bearing jarosite would likely enhance the conclusion of Navrotsky et al. (2005) that once jarosite formed it could remain stable on the Martian surface as a component in the dust and soil.

If abundant deliquescent phases such as molysite were added to the martian surface during magma degassing, transient liquid brines could have periodically formed that would have incorporated much of the soluble material that was deposited by magmatic vapor. If terrestrial analogs are good indicators of brines like these, they would be quite acidic (Benison & LaClair, 2003). This is seemingly difficult to reconcile with the proposed abundance of carbonate (2-5 wt.%) in Martian fines (Bandfield et al., 2003). However, it must be noted that the carbonates are most likely formed in aqueous processes that are independent from those involved in mineral deposition from magmatic degassing. Thus, it is possible that mechanical mixing of carbonate and the evaporative products of the brine and could be incorporated into the global dust layer.

5.3. How Much Material Could Have Been Added to the Martian Surface by This Process?

Recent Martian volcanism identified at Elysium (Plescia, 1993; Vaucher et al., 2009), Olympus Mons (Chadwick et al., 2015; Mangold et al., 2010), and other locales on the surface (Hauber et al., 2011) could have given rise to vapor-deposited minerals similar to what we obtained experimentally. An important question remains regarding how much material this process could have contributed to the surface. Quantification of the amount of vapor-deposited material formed from a cooling lava is not a straightforward process as it will depend upon the gas/melt ratio, the composition of the gas, and factors such as the area of the depositional surfaces. The gas/melt ratio may be much higher than that expected from simple volatile solubility limits (e.g., Filiberto & Treiman, 2009; Gaillard & Scaillet, 2009; Righter et al., 2009). Wallace (2001) showed that terrestrial volcanic systems release on average 10 times more SO_2 than can be accounted for by the erupted volumes of lava and attributed this to formation of a vapor phase at depth and migration of this phase upward though the magma plumbing system. As these bubbles of gas concentrate, they effectively enrich the upper portions of the magma chamber with exsolved gas. With the higher abundance of Cl and S and the lower amount of water in late Martian magmas relative to terrestrial magmas (Filiberto & Treiman, 2009; Filiberto, Baratoux, et al., 2016; Filiberto, Gross, et al., 2016), the amount of sublimates arising from passive degassing flows may be much higher than from terrestrial lava flows where water and CO_2 remain the dominant gases released.

When considering that Martian magmas appear to inherit up to 0.3 wt.% Cl (Filiberto & Treiman, 2009), and up to 0.4 wt % (Righter et al., 2009) or 1.2 wt.% S (Gaillard & Scaillet, 2009) from their source, the concentrations of these volatiles in our experiments did not produce an unreasonably high gas/melt ratio. The experiments therefore can be used to provide a rough estimate of the sublimate load that could have been added to the surface by recent Martian lava flows. Our estimation is necessarily simplified and takes the weight of sublimates relative to the weight of glass source to determine the relative amount of sublimates produced. The experiments show that between 1.9 wt% (for the I(Cl+S) composition) and 3.7 wt% (for the I(Cl+HiS) composition) of the mass of the source glass was converted to the precipitates observed. [The actual mass transported from the melt was higher than this since it would have included vapor phase components that did not precipitate a solid phase, such as SO_2 and H_2O.]

Table 5 shows estimated quantities of vapor-deposited minerals contributed to the surface by recent igneous activity Mars. The calculations assume (i) that the vapor-deposited minerals from a lava of Irvine composition is a reasonable analog for other Martian magmas and the initial volatile load at depth is similar to that of the experiments, (ii) that 2 wt% of the lava mass is converted to vapor-deposited minerals as per the lower value of the experiments, (iii) that the density of the lava is 3,000 kg/m^3 and that of the vapor-deposited material is 4,000 kg/m^3 (roughly intermediate between chlorides, sulfides, and oxides). The computed thickness of global coverage by vapor deposits contributed by young volcanism (Table 5) is markedly similar to the thicknesses predicted by Franz et al. (2018); however, their computations assumed the formation of vapor-deposited sulfate rather than the sulfides and chlorides observed here, with young Olympus Mons eruptions alone producing enough vapor-deposited material to blanket the planet to a thickness of 15 cm.

Although young volcanism is expected to have made a major contribution of Cl and S to the present-day dust though vapor-deposited material, these contributions may be masked by contributions from older fine-

Table 5
Computed Amount of Vapor-deposited Material Potentially Contributed to the Martian Surface by Young Extrusive Rocks

Location	Age (Ma)	Lava Vol (km^3)	Lava Mass[f] (kg)	Vapor-deposits mass[g] (kg)	Vapor-deposits vol (km^3)	Global coverage (m)
Arsia Mons	10-250[a]	3.3E+03[a]	9.90E+15	1.98E+14	49.5	3.40E−04
Central Elysium Planitia	2-250[b]	1.7E+05[b]	5.10E+17	1.02E+16	2,550	0.02
Olympus Mons	170-250[c]	1.4E+06[c]	4.20E+18	8.40E+16	21,000	0.15
Medusae Fossae Formation	Hesperian/Amazonian[d]	1.4E+06[e]	4.20E+18	8.40E+16	21,000	0.15

[a]Richardson et al. (2017). [b]Vaucher et al. (2009). [c]Chadwick et al. (2015). [d]Kerber and Head (2010). [e]Bradley et al. (2002). [f]Assuming a magma density of 3,000 kg/m^3. [g]Assuming a vapor deposit density of 4,000 kg/m^3.

grained formations susceptible to aeolian weathering. This can probably be best exemplified by the Medusae Fossae Formation (MFF). Although the recent volcanism from Olympus Mons could have contributed just as much vapor-deposited material as the MFF (Table 5), Ojha et al. (2018) noted that the MFF provides the best chemical match to surface measurements of Martian dust. The MFF has been considered an easily erodible pyroclastic deposit and it is possible that its high Cl and S is due to vapor-deposited material on the surface of the ash. The absence of sulfates in this unit (Ojha et al., 2018) suggests that the prime contribution of Cl and S is through the formation of vapor-deposited sulfides, native sulfur, and chlorides rather than by interaction of the glass and magmatic gas to form sulfates.

6. Conclusions

Experiments conducted using a typical Martian basalt have demonstrated that when a lava enriched in a OH-poor, S-, and Cl-rich gas cools on the Martian surface, the magmatic vapors may condense to form micron-sized particles of halite, lawrencite, sylvite, silica, magnetite, pyrrhotite, pyrite, and sulfur over a range of temperatures between approximately 700 and 100°C. These phases can oxidize or react with the cooling gas to form a variety of secondary phases including molysite, maghemite, hematite, iron oxychloride, and possibly jarosite, akaganéite, and perchlorates, all of which could be incorporated into the Martian dust and widely distributed. The fines on the modern surface of Mars may have seen a large contribution of what was originally vapor-deposited phases from gases from low-OH magmas.

Acknowledgments
We would like to acknowledge the NASA Mars Fundamental Research and NSF Geochemistry and Petrology programs for providing the funding for this study. We would also like to thank Donald Lindsley for helpful discussions on oxide equilibria, James Quinn for his help with SEM analysis, and the American Museum of Natural History for the use of their electron microprobe. All data obtained in this study and the experimental and analytical methods used are presented within the body of the text and in tables. Physical products of the work are curated by H. Nekvasil and available upon request.

References

Africano, F., Van Rompaey, G., Bernard, A., & Le Guern, F. (2002). Deposition of trace elements from high temperature gases of Satsuma-Iwojima volcano. *Earth, Planets and Space*, *54*, 275–286. https://doi.org/10.1186/BF03353027

Andersen, D. J., Lindsley, D. H., & Davidson, P. M. (1993). QUILF: A Pascal program to assess equilibria among Fe, Mg, Mn, Ti- oxides, pyroxenes, olivine, and quartz. *Computers and Geosciences*, *19*(9), 1333–1350. https://doi.org/10.1016/0098-3004(93)90033-2

Argo, J. (1981). On the nature of 'ferrous' corrosion products on marine iron. *Studies in Conservation*, *26*, 42–44. https://doi.org/10.1179/sic.1981.26.1.42

Atreya, S. K., Wong, A. S., Renno, N. O., Farrell, W. M., Delory, G. T., Sentman, D. D., et al. (2006). Oxidant enhancement in Martian dust devils and storms: Implications for life and habitability. *Astrobiology*, *6*(3), 439–450. https://doi.org/10.1089/ast.2006.6.439

Aubaud, C., Hauri, E. H., & Hirschmann, M. M. (2004). Hydrogen partition coefficients between nominally anhydrous minerals and basaltic melts. *Geophysical Research Letters*, *31*, L20611. https://doi.org/10.1029/2004GL021341

Baird, A. K., Toulmin, P., Clark, B. C., Rose, H. J., Keil, K., Christian, R. P., & Gooding, J. L. (1976). Mineralogic and petrologic implications of Viking geochemical results from Mars: Interim report. *Science*, *194*(4271), 1288–1293. https://doi.org/10.1126/science.194.4271.1288

Bandfield, J. L., Glotch, T. D., & Christensen, P. R. (2003). Spectroscopic Identification of Carbonate Minerals in the Martian Dust. *Science*, *301*(5636), 1084–1087. https://doi.org/10.1126/science.1088054

Banin, A., Ben-Shlomo, T., Margulies, L., Blake, D. F., Mancinelli, R. L., & Gehring, A. U. (1993). The nanophase iron mineral(s) in Mars soil. *Journal of Geophysical Research*, *98*(E11), 20,831–20,853. https://doi.org/10.1029/93JE02500

Barron, V., & Torrent, J. (2002). Evidence for a simple pathway to maghemite in Earth and Mars soils. *Geochimica et Cosmochimica Acta*, *66*(15), 2801–2806. https://doi.org/10.1016/S0016-7037(02)00876-1

Benison, K. C., & LaClair, D. A. (2003). Modern and ancient extremely acid saline deposits: terrestrial analogs for Martian environments? *Astrobiology*, *3*(3), 609–618. https://doi.org/10.1089/153110703322610690

Benoit, M. H., Nyblade, A. A., & VanDecar, J. C. (2006). Upper mantle P-wave speed variations beneath Ethiopia and the origin of the Afar hot spot. *Geology*, *34*(5), 329–332. https://doi.org/10.1130/G22281.1

Berger, J. A., Schmidt, M. E., Gellert, R., Campbell, J. L., King, P. L., Flemming, R. L., et al. (2016). A global Mars dust composition refined by the Alpha Particle X-ray Spectrometer in Gale Crater. *Geophysical Research Letters*, *43*, 67–75. https://doi.org/10.1002/2015GL066675

Bernard, A., & Le Guern, F. (1986). Condensation of volatile elements in high-temperature gases of Mount St. Helens. *Journal of Volcanology and Geothermal Research*, *28*, 91–105. https://doi.org/10.1016/0377-0273(86)90007-7

Bertelsen, P., Goetz, W., Madsen, M. B., Kinch, K. M., Hviid, S. F., Knudsen, J. M., & Bell, J. F. (2004). Magnetic properties experiments on the Mars Exploration Rover Spirit at Gusev crater. *Science*, *305*(5685), 827–829. https://doi.org/10.1126/science.1100112

Bibring, J. P., Squyres, S. W., & Arvidson, R. E. (2006). Merging views on Mars. *Science*, *313*(5795), 1899–1901. https://doi.org/10.1126/science.1132311

Bluth, G. J., Scott, C. J., Sprod, I. E., Schnetzler, C. C., Krueger, A. J., & Walter, L. S. (1995). Explosive emissions of sulfur dioxide from the 1992 Crater Peak eruptions, Mount Spurr volcano, Alaska. In T. E. C. Keith (Ed.), *The 1992 eruptions of Crater Peak vent, Mount Spurr volcano, Alaska. United States Geological Survey Bulletin*, (Vol. 2139, pp. 37–40). Washington, DC: Government Printing Office.

Bogatyrev, A. F., Makeenkova, O. A., & Nezovitina, M. A. (2014). Temperature and concentration dependences of thermal-diffusion separation in ternary gas systems. *Journal of Engineering Physics and Thermophysics*, *87*(5), 1255–1265. https://doi.org/10.1007/s10891-014-1128-8

Bradley, B. A., Sakimoto, S. E. H., Frey, H., & Zimbelman, J. R. (2002). Medusae Fossae Formation: New perspectives from Mars Global Surveyor. *Journal of Geophysical Research*, *107*(E8), 5058. https://doi.org/10.1029/2001JE001537

Buddington, A. F., & Lindsley, D. H. (1964). Iron-titanium oxide minerals and synthetic equivalents. *Journal of Petrology*, *5*(2), 310–357. https://doi.org/10.1093/petrology/5.2.310

Burns, R. G., & Fisher, D. S. (1990). Iron-sulfur mineralogy of Mars: Magmatic evolution and chemical weathering products. *Journal of Geophysical Research*, *95*(B9), 14,415–14,421. https://doi.org/10.1029/JB095iB09p14415

Carrier, B. L., & Kounaves, S. P. (2015). The origins of perchlorate in the Martian soil. *Geophysical Research Letters*, *42*, 3739–3745. https://doi.org/10.1002/2015GL064290

Chadwick, J., McGovern, P., Simpson, M., & Reeves, A. (2015). Late Amazonian subsidence and magmatism of Olympus Mons, Mars. *Journal of Geophysical Research: Planets*, *120*, 1585–1595. https://doi.org/10.1002/2015JE004875

Chapman, S., & Cowling, T. G. (1953). *The mathematical theory of non-uniform gases: Notes added in 1951*. Cambridge, England: Cambridge University Press.

Chapman, S., & Dootson, F. W. (1917). XXII. A note on thermal diffusion. *The London, Edinburgh, and Dublin Philosophical Magazine and Journal of Science*, *33*, 248–253. https://doi.org/10.1080/14786440308635635

Chase, M. W. Jr. (1998). NIST-JANAF Thermochemical Tables. In *Journal of Physical and Chemistry Reference Data*, *Monograph*, (Fourth ed., Vol. 9). Gaithersburg, Maryland: National Institute of Standards and Technology.

Chevrier, V., & Mathé, P. E. (2007). Mineralogy and evolution of the surface of Mars: a review. *Planetary and Space Science*, *55*, 289–314. https://doi.org/10.1016/j.pss.2006.05.039

Chouinard, A., Williams-Jones, A. E., Leonardson, R. W., Hodgson, C. J., Silva, P., Téllez, C., et al. (2005). Geology and genesis of the multistage high-sulfidation epithermal Pascua Au-Ag-Cu deposit, Chile and Argentina. *Economic Geology*, *100*(3), 463–490. https://doi.org/10.2113/gsecongeo.100.3.463

Clark, B. C., & Baird, A. K. (1979). Is the Martian lithosphere sulfur rich? *Journal of Geophysical Research*, *84*, 8395–8403. https://doi.org/10.1029/JB084iB14p08395

Clark, B. C., Baird, A. K., Rose, H. J., Toulmin, P., Christian, R. P., Kelliher, W. C., et al. (1977). The Viking X ray fluorescence experiment: Analytical methods and early results. *Journal of Geophysical Research*, *82*(28), 4577–4594. https://doi.org/10.1029/JS082i028p04577

Clark, B. C., Baird, A. K., Weldon, R. J., Tsusaki, D. M., Schnabel, L., & Candelaria, M. P. (1982). Chemical composition of Martian fines. *Journal of Geophysical Research*, *87*, 10,059–10,067. https://doi.org/10.1029/JB087iB12p10059

Clark, B. C., & Van Hart, D. C. (1981). The salts of Mars. *Icarus*, *45*(2), 370–378. https://doi.org/10.1016/0019-1035(81)90041-5

Cumplido, J., Barrón, V., & Torrent, J. (2000). Effect of phosphate on the formation of nanophase lepidocrocite from Fe (II) sulfate. *Clays and Clay Minerals*, *48*(5), 503–510. https://doi.org/10.1346/CCMN.2000.0480502

Dai, Y. D., Yu, Z., Huang, H. B., He, Y., Shao, T., & Hsia, Y. F. (2003). Thermal decomposition of iron oxychloride as studied by thermal analysis, X-ray diffraction and Mössbauer spectroscopy. *Materials Chemistry and Physics*, *79*, 94–97. https://doi.org/10.1016/S0254-0584(02)00449-2

de Moor, J. M., Fischer, T. P., Sharp, Z. D., King, P. L., Wilke, M., Botcharnikov, R. E., & Rivard, C. (2013). Sulfur degassing at Erta Ale (Ethiopia) and Masaya (Nicaragua) volcanoes: Implications for degassing processes and oxygen fugacities of basaltic systems. *Geochemistry, Geophysics, Geosystems*, *14*, 4076–4108.

Deen, W. M. (2013). *Analysis of transport phenomena*. Oxford, England: Oxford University Press.

Dixon, J. E., Stolper, E. M., & Holloway, J. R. (1995). An experimental study of water and carbon dioxide solubilities in mid-ocean ridge basaltic liquids. Part I: calibration Calibration and solubility models. *Journal of Petrology*, *36*, 1607–1631. https://doi.org/10.1093/oxfordjournals.petrology.a037267

Dutrizac, J. E. (2008). Factors affecting the precipitation of potassium jarosite in sulfate and chloride media. *Metallurgical and Materials Transactions B*, *39*, 771–783. https://doi.org/10.1007/s11663-008-9198-7

Filiberto, J., Baratoux, D., Beaty, D., Breuer, D., Farcy, B. J., Grott, M., et al. (2016). A review of volatiles in the Martian interior. *Meteoritics & Planetary Science*, *51*(11), 1935–1958. https://doi.org/10.1111/maps.12680

Filiberto, J., Gross, J., & McCubbin, F. M. (2016). Constraints on the water, chlorine, and fluorine content of the Martian mantle. *Meteoritics & Planetary Science*, *51*(11), 2023–2035. https://doi.org/10.1111/maps.12624

Filiberto, J., Treiman, A. H., Giesting, P.A., Goodrich, C. A., & Gross, J. (2014). High-temperature chlorinerich fluid in the Martian crust: a precursor to habitability. *Earth & Planetary Science Letters*, *401*, 110-115, DOI: https://doi.org/10.1016/j.epsl.2014.06.003.

Filiberto, J., & Treiman, A. H. (2009). Martian magmas contained abundant chlorine, but little water. *Geology*, *37*, 1087–1090. https://doi.org/10.1130/G30488A.1

Franz, H., King, P. L., & Gaillard, F. (2018). Sulfur on Mars from the atmosphere to the core. In J. Filiberto, & S. P. Schwenzer (Eds.), *Volatiles in the Martian Crust*. (Chap. 6, pp. 119-183). New York, NY: Elsevier.

Gaillard, F., & Scaillet, B. (2009). The sulfur content of volcanic gases on Mars. *Earth and Planetary Science Letters*, *279*, 34–43. https://doi.org/10.1016/j.epsl.2008.12.028

Gaillard, F., Michalski, J., Berger, G., McLennan, S. M., & Scaillet, B. (2013). Geochemical reservoirs and timing of sulfur cycling on Mars. *Space Science Reviews*, *174*, 251–300. https://doi.org/10.1007/s11214-012-9947-4

Gellert, R., Rieder, R., Anderson, R. C., Brückner, J., Clark, B. C., Dreibus, G., et al. (2004). Chemistry of rocks and soils in Gusev Crater from the Alpha Particle X-ray Spectrometer. *Science*, *305*(5685), 829–832. https://doi.org/10.1126/science.1099913

Gellert, R., Rieder, R., Brückner, J., Clark, B. C., Dreibus, G., Klingelhöfer, G., et al. (2006). Alpha particle X-ray spectrometer (APXS): Results from Gusev crater and calibration report. *Journal of Geophysical Research*, *111*(E2). https://doi.org/10.1029/2005JE002555

Ghiorso, M. S., & Sack, R. O. (1995). Chemical mass transfer in magmatic processes IV. A revised and internally consistent thermodynamic model for the interpolation and extrapolation of liquid-solid equilibria in magmatic systems at elevated temperatures and pressures. *Contributions to Mineralogy and Petrology*, *119*, 197–212. https://doi.org/10.1007/BF00307281

Giesting, P. A., & Filiberto, J. (2016). The formation environment of potassic-chloro-hastingsite in the nakhlites MIL 03346 and pairs and NWA 5790: Insights from terrestrial chloro-amphibole. *Meteoritics & Planetary Science*, *51*(11), 2127–2153. https://doi.org/10.1111/maps.12675

Gillespie, L. J. (1939). A simple theory for separation of gases by thermal diffusion. *The Journal of Chemical Physics*, *7*(7), 530–535. https://doi.org/10.1063/1.1750482

Glavin, D. P., Freissinet, C., Miller, K. E., Eigenbrode, J. L., Brunner, A. E., Buch, A., et al. (2013). Evidence for perchlorates and the origin of chlorinated hydrocarbons detected by SAM at the Rocknest aeolian deposit in Gale Crater. *Journal of Geophysical Research: Planets*, *118*, 1955–1973. https://doi.org/10.1002/jgre.20144

Glotch, T. D., Bandfield, J. L., Wolff, M. J., Arnold, J. A., & Che, C. (2016). Constraints on the composition and particle size of chloride salt-bearing deposits on Mars. *Journal of Geophysical Research: Planets*, *121*, 454–471. https://doi.org/10.1002/2015JE004921

Gooding, J. L. (1978). Chemical weathering on Mars thermodynamic stabilities of primary minerals (and their alteration products) from mafic igneous rocks. *Icarus*, *33*(3), 483–513.

Gooding, J. L., Arvidson, R. E., & Zolotov, M. (1992). Physical and chemical weathering. In H. H. Kieffer (Ed.), Mars (pp. 626-651). University of Arizona Press, Space Science Series.

Gorban, A. N., Sargsyan, H. P., & Wahab, H. A. (2011). Quasichemical models of multicomponent nonlinear diffusion. *Mathematical Modelling of Natural Phenomena*, *6*(5), 184–262. https://doi.org/10.1051/mmnp/20116509

Gough, R. V., Chevrier, V. F., & Tolbert, M. A. (2014). Formation of aqueous solutions on Mars via deliquescence of chloride–perchlorate binary mixtures. *Earth and Planetary Science Letters*, *393*, 73–82. https://doi.org/10.1016/j.epsl.2014.02.002

Gough, R. V., Chevrier, V. F., & Tolbert, M. A. (2016). Formation of liquid water at low temperatures via the deliquescence of calcium chloride: Implications for Antarctica and Mars. *Planetary and Space Science*, *131*, 79–87. https://doi.org/10.1016/j.pss.2016.07.006

Hahn, B. C., & McLennan, S. M. (2010). Sediments and the chemical composition of the upper Martian crust. In *First International Conference on Mars Sedimentology and Stratigraphy*, Abstract # 30. Lunar and Planetary Institute publication

Halbert, T. R., Johnston, D. C., McCandlish, L. E., Thompson, A. H., Scanlon, J. C., & Dumesic, J. A. (1980). Intercalation of organometallic compounds into layered transition metal oxyhalides. *Physica B + C*, *38*(10), 128–132. https://doi.org/10.1029/2011GL047310

Hauber, E., Brož, P., Jagert, F., Jodłowski, P., & Platz, T. (2011). Very recent and wide-spread basaltic volcanism on Mars. *Geophysical Research Letters*, *38*, L10201. https://doi.org/10.1029/2011GL047310

Hecht, M. H., Kounaves, S. P., Quinn, R. C., West, S. J., Young, S. M. M., Ming, D. W., et al. (2009). Detection of perchlorate and the soluble chemistry of Martian soil at the Phoenix lander site. *Science*, *325*(5936), 64–67. https://doi.org/10.1126/science.1172466

Henley, R. W., & Seward, T. M. (2018). Gas-solid reactions in Arc Volcanoes: Ancient and Modern. High Temperature Gas-solid Reactions in Earth and Planetary Processes. In P. L. King, B. Fegley, & T. Seward (Eds.), *Reviews in Mineralogy and Geochemistry, Mineralogical Society of America* (Vol. 84) Virginia: Chantilly.

Herd, C. D. (2006). Insights into the redox history of the NWA 1068/1110 Martian basalt from mineral equilibria and vanadium oxybarometry. *American Mineralogist*, *91*(10), 1616–1627. https://doi.org/10.2138/am.2006.2104

Herd, C. D., Papike, J. J., & Brearley, A. J. (2001). Oxygen fugacity of Martian basalts from electron microprobe oxygen and TEM-EELS analyses of Fe-Ti oxides. *American Mineralogist*, *86*(9), 1015–1024. https://doi.org/10.2138/am-2001-8-908

Herd, C. D. K., Walton, E. L., Agee, C. B., Muttik, N., Ziegler, K., Shearer, C. K., et al. (2017). The Northwest Africa 8159 Martian meteorite: Expanding the Martian sample suite to the early Amazonian. *Geochimica et Cosmochimica*, *218*, 1–26. https://doi.org/10.1016/j.gca.2017.08.037

Hogancamp, V. J., Sutter, B., Morris, V. R., Archer, D. P., Ming, D. W., Rampe, E., et al. (2018). Chlorate/Fe-bearing phase mixtures as a possible source of oxygen and chlorine detected by the sample analysis at Mars (SAM) instrument in Gale Crater, Mars. *Journal of Geophysical Research: Planets*, *123*(11), 2920–2938. https://doi.org/10.1029/2018JE005691

Hynek, B. M., Osterloo, M. K., & Kierein-Young, K. S. (2015). Late-stage formation of Martian chloride salts through ponding and evaporation. *Geology*, *43*, 787–790. https://doi.org/10.1130/G36895.1

Joachim, B., Pawley, A., Lyon, I. C., Marquardt, K., Henkel, T., Clay, P. L., et al. (2015). Experimental partitioning of F and Cl between olivine, orthopyroxene and silicate melt at Earth's mantle conditions. *Chemical Geology*, *416*, 65–78. https://doi.org/10.1016/j.chemgeo.2015.08.012

Johnson, E. R., Wallace, P. J., Cashman, K. V., & Granados, H. D. (2010). Degassing of volatiles (H_2O, CO_2, S, Cl) during ascent, crystallization, and eruption at mafic monogenetic volcanoes in central Mexico. *Journal of Volcanology and Geothermal Research*, *197*, 225–238. https://doi.org/10.1016/j.jvolgeores.2010.02.017

Johnson, M. C., Rutherford, M. J., & Hess, P. C. (1991). Chassigny petrogenesis: Melt compositions, intensive parameters and water contents of Martian (?) magmas. *Geochimica et Cosmochimica Acta*, *55*, 349–366. https://doi.org/10.1016/0016-7037(91)90423-3

Jubb, A. M., & Allen, H. C. (2010). Vibrational spectroscopic characterization of hematite, maghemite, and magnetite thin films produced by vapor deposition. *ACS Applied Materials & Interfaces*, *2*, 2804–2812. https://doi.org/10.1021/am1004943

Jugo, J., Wilke, M., & Botcharnikov, R. E. (2010). Sulfur K-edge XANES analysis of natural and synthetic basaltic glasses: Implications for S speciation and S content as a function of oxygen fugacity. *Geochimica et Cosmochimica Acta*, *74*(20), 5926–5938. https://doi.org/10.1016/j.gca.2010.07.022

Kanungo, S. B., & Mishra, S. K. (1997). Kinetics of chloridization of nickel-bearing lateritic iron ore by hydrogen chloride gas. *Metallurgical and Materials Transactions B*, *28*, 389–399. https://doi.org/10.1007/s11663-997-0104-5

Keller, J. M., Boynton, W. V., Karunatillake, S., Baker, V. R., Dohm, J. M., Evans, L. G., et al. (2006). Equatorial and midlatitude distribution of chlorine measured by Mars Odyssey GRS. *Journal of Geophysical Research*, *112*(E3), 111. https://doi.org/10.1029/2006JE002679

Kerber, L., & Head, J. W. (2010). The age of the Medusae Fossae Formation: Evidence of Hesperian emplacement from crater morphology, stratigraphy, and ancient lava contacts. *Icarus*, *206*(2), 669–684. https://doi.org/10.1016/j.icarus.2009.10.001

Kiefer, W. S., Filiberto, J., Sandu, C., & Li, Q. (2015). The effects of mantle composition on the peridotite solidus: Implications for the magmatic history of Mars. *Geochimica et Cosmochimica Acta*, *162*, 247–258. https://doi.org/10.1016/j.gca.2015.02.010

King, P. L., Lescinsky, D. T., & Nesbitt, H. W. (2004). The composition and evolution of primordial solutions on Mars, with application to other planetary bodies. *Geochimica et Cosmochimica Acta*, *68*(23), 4993–5008. https://doi.org/10.1016/j.gca.2004.05.036

King, P. L., & McLennan, S. M. (2010). Sulfur on Mars. *Elements*, *6*(2), 107–112. https://doi.org/10.2113/gselements.6.2.107

King, P. L., & McSween, H. Y. Jr. (2005). Effects of H_2O, pH, and oxidation state on the stability of Fe minerals on Mars. *Journal of Geophysical Research*, *110*, E12S10. https://doi.org/10.1029/2005JE002482

King, P. L., Wheeler, V. W., Renggli, C. J., Palm, A. B., Wilson, S., Harrison, P., et al. (2018). Gas-solid reactions: Theory, experiments and case studies relevant to Earth and planetary processes. *Reviews in Mineralogy and Geochemistry*, *84*(1), 1–56. https://doi.org/10.2138/rmg.2018.84.1

Kounaves, S. P., Carrier, B. L., O'Neil, G. D., Stroble, S. T., & Claire, M. W. (2014). Evidence of Martian perchlorate, chlorate, and nitrate in Mars meteorite EETA79001: Implications for oxidants and organics. *Icarus*, *229*, 206–213. https://doi.org/10.1016/j.icarus.2013.11.012

Krauskopf, K. B. (1957). The heavy metal content of magmatic vapor at 600°C. *Economic Geology*, *52*, 786–807. https://doi.org/10.2113/gsecongeo.52.7.786

Krauskopf, K. B. (1964). The possible role of volatile metal compounds in ore genesis. *Economic Geology*, *59*, 22–45. https://doi.org/10.2113/gsecongeo.59.1.22

Leshin, L. A., Mahaffy, P. R., Webster, C. R., Cabane, M., Coll, P., Conrad, P. G., et al. (2013). Volatile, isotope, and organic analysis of Martian fines with the Mars Curiosity rover. *Science*, *341*(6153), 1238937. https://doi.org/10.1126/science.1238937

Lindsley, D. H. (1976). Experimental studies of oxide minerals. In D. Rumble, III (Ed.), *Oxide Minerals, MSA Short Course Notes*, (Vol. 3, pp. L-61–L-88). Washington, DC, Mienraological Society of America.

Madsen, M. B., Hviid, S. F., Gunnlaugsson, H. P., Knudsen, J. M., Goetz, W., Pedersen, C. T., et al. (1999). The magnetic properties experiments on Mars Pathfinder. *Journal of Geophysical Research*, *104*(E4), 8761–8779. https://doi.org/10.1029/1998JE900006

Mandeville, C. W., Webster, J. D., Rutherford, M. J., Taylor, B. E., Timbal, A., & Faure, K. (2002). Determination of molar absorptivities for infrared absorption bands of H_2O in andesitic glasses. *American Mineralogist*, *87*, 813–821. https://doi.org/10.2138/am-2002-0702

Mangold, N., Loizeau, D., Poulet, F., Ansan, V., Baratoux, D., LeMouelic, S., et al. (2010). Mineralogy of recent volcanic plains in the Tharsis region, Mars, and implications for platy-ridged flow composition. *Earth and Planetary Science Letters*, *294*(3-4), 440–450. https://doi.org/10.1016/j.epsl.2009.07.036

Mather, T. A., Allen, A. G., Oppenheimer, C., Pyle, D. M., & McGonigle, A. J. S. (2003). Size-resolved characterisation of soluble ions in the particles in the tropospheric plume of Masaya volcano, Nicaragua: Origins and plume processing. *Journal of Atmospheric Chemistry*, *46*, 207–237. https://doi.org/10.1023/A:102632750

McCollom, T. M., & Hynek, B. M. (2005). A volcanic environment for bedrock diagenesis at Meridiani Planum on Mars. *Nature*, *438*, 1129. https://doi.org/10.1038/nature04390

McCubbin, F. M., Boyce, J. W., Novák-Szabó, T., Santos, A. R., Tartèse, R., Muttik, N., et al. (2016). Geologic history of Martian regolith breccia Northwest Africa 7034: Evidence for hydrothermal activity and lithologic diversity in the Martian crust. *Journal of Geophysical Research: Planets*, *121*, 2120–2149. https://doi.org/10.1002/2016JE005143

McCubbin, F. M., & Nekvasil, H. (2008). Maskelynite-hosted apatite in the Chassigny meteorite: Insights into late-stage magmatic volatile evolution in Martian magmas. *American Mineralogist*, *93*, 676–684. https://doi.org/10.2138/am.2008.2558

McCubbin, F. M., Tosca, N. J., Smirnov, A., Nekvasil, H., Steele, A., Fries, M., & Lindsley, D. H. (2009). Hydrothermal jarosite and hematite in a pyroxene-hosted melt inclusion in Martian meteorite MIL 03346: Implications for magmatic hydrothermal fluids on Mars. *Geochimica et Cosmochimica Acta*, *73*(16), 4907–4917. https://doi.org/10.1016/j.gca.2009.05.031

McLennan, S. M., Anderson, R. B., Bell, J. F. III, Bridges, J. C., Calef, F. III, Campbell, J. L., et al., & MSL Science Team (2014). Elemental geochemistry of sedimentary rocks in Yellowknife Bay, Gale Crater, Mars. *Science*, *343*(6169), 1244734. https://doi.org/10.1126/science.1244734

McSween, H. Y. (1994). What we have learned about Mars from SNC meteorites. *Meteoritics and Planetary Science*, *29*, 757–779. https://doi.org/10.1111/j.1945-5100.1994.tb01092.x

McSween, H. Y., Wyatt, M. B., Gellert, R., Bell, J. F., Morris, R. V., Herkenhoff, K. E., et al. (2006). Characterization and petrologic interpretation of olivine-rich basalts at Gusev Crater, Mars. *Journal of Geophysical Research*, *111*(E2), E2. https://doi.org/10.1029/2005JE002477

Ming, D. W., Archer, P. D., Glavin, D. P., Eigenbrode, J. L., Franz, H. B., Sutter, B., et al. (2014). Volatile and organic compositions of sedimentary rocks in Yellowknife Bay, Gale Crater, Mars. *Science*, *343*(6169), 1245267. https://doi.org/10.1126/science.1245267

Morris, R. V., Bristow, T. F., Rampe, E. B., Yen A. S., Vaniman, D. T., Tu, V., et al. (2019) Mineralogy and formation processes for the-Vera Rubin Ridge at Gale crater, Mars, from CHEMIN XRD analyses. 50th LPSC, Abstract # 1127.

Morris, R. V., Golden, D. C., Bell, J. F., Shelfer, T. D., Scheinost, A. C., Hinman, N. W., et al. (2000). Mineralogy, composition, and alteration of Mars Pathfinder rocks and soils: Evidence from multispectral, elemental, and magnetic data on terrestrial analogue, SNC meteorite, and Pathfinder samples. *Journal of Geophysical Research*, *105*(E1), 1757–1817. https://doi.org/10.1029/1999JE001059

Morris, R. V., Golden, D. C., Ming, D. W., Shelfer, T. D., Jørgensen, L. C., Bell, J. F., et al. (2001). Phyllosilicate-poor palagonitic dust from Mauna Kea Volcano (Hawaii): A mineralogical analogue for magnetic Martian dust? *Journal of Geophysical Research*, *106*(E3), 5057–5083. https://doi.org/10.1029/2000JE001328

Morris, R. V., Golden, D. C., Shelfer, T. D., & Lauer, H. V. (1998). Lepidocrocite to maghemite to hematite: a pathway to magnetic and hematitic Martian soil. *Meteoritics and Planetary Science*, *33*, 743–751. https://doi.org/10.1111/j.1945-5100.1998.tb01680.x

Morris, R. V., Klingelhoefer, G., Schröder, C., Rodionov, D. S., Yen, A., Ming, D. W., et al. (2006). Mössbauer mineralogy of rock, soil, and dust at Gusev crater, Mars: Spirit's journey through weakly altered olivine basalt on the plains and pervasively altered basalt in the Columbia Hills. *Journal of Geophysical Research*, *111*(E2), 111. https://doi.org/10.1029/2005JE002584

Nachon, M., Clegg, S. M., Mangold, N., Schröder, S., Kah, L. C., Dromart, G., et al. (2014). Calcium sulfate veins characterized by ChemCam/Curiosity at Gale crater, Mars. *Journal of Geophysical Research: Planets*, *119*, 1991–2016. https://doi.org/10.1002/2013JE004588

Navrotsky, A., Forray, F. L., & Drouet, C. (2005). Jarosite stability on Mars. *Icarus*, *176*(1), 250–253. https://doi.org/10.1016/j.icarus.2005.02.003

Niles, P. B., & Michalski, J. (2009). Meridiani Planum sediments on Mars formed through weathering in massive ice deposits. *Nature Geoscience*, *2*, 215. https://doi.org/10.1038/ngeo438

Nuding, D. L., Rivera-Valentin, E. G., Davis, R. D., Gough, R. V., Chevrier, V. F., & Tolbert, M. A. (2014). Deliquescence and efflorescence of calcium perchlorate: An investigation of stable aqueous solutions relevant to Mars. *Icarus*, *243*, 420–428. https://doi.org/10.1016/j.icarus.2014.08.036

Ojha, L., Lewis, K., Karunatillake, S., & Schmidt, M. (2018). The Medusae Fossae Formation as the single largest source of dust on Mars. *Nature Communications*, *9*, 2867. https://doi.org/10.1038/s41467-018-05291-5

Osterloo, M. M., Anderson, F. S., Hamilton, V. E., & Hynek, B. M. (2010). Geologic context of proposed chloridebearing materials on Mars. *Journal of Geophysical Research*, 115. https://doi.org/10.1029/2010JE003613

Osterloo, M. M., Hamilton, V. E., Bandfield, J. L., Glotch, T. D., Baldridge, A. M., & Christensen, et al. (2008). Chloride-bearing materials in the southern highlands of Mars. *Science*, *319*, 1651–1654. https://doi.org/10.1126/science.1150690

Patrick, M. R., Dehn, J., & Dean, K. (2004). Numerical modeling of lava flow cooling applied to the 1997 Okmok eruption: Approach and analysis. *Journal of Geophysical Research*, *109*, B03202. https://doi.org/10.1029/2003JB002537

Platten, J. K. (2006). The Soret effect: A review of recent experimental results. *Journal of Applied Mechanics*, *73*(1), 5–15. https://doi.org/10.1115/1.1992517

Plescia, J. B. (1993). An assessment of volatile release from recent volcanism in Elysium, Mars. *Icarus*, *104*, 20–32. https://doi.org/10.1006/icar.1993.1079

Pokrovski, G. S., Borisova, A. Y., & Bychkov, A. Y. (2013). Speciation and transport of metals and metalloids in geological vapors. *Reviews in Mineralogy and Geochemistry*, *76*(1), 165–218. https://doi.org/10.2138/rmg.2013.76.6

Renggli, C. J., King, P. L., Henley, R. W., & Norman, M. D. (2017). Volcanic gas composition, metal dispersion and deposition during explosive volcanic eruptions on the Moon. *Geochimica et Cosmochimica Acta*, *206*, 296–311. https://doi.org/10.1016/j.gca.2017.03.012

Richardson, J. A., Wilson, J. A., Connor, C. B., Bleacher, J. E., & Kiyosugi, K. (2017). Recurrence rate and magma effusion rate for the latest volcanism on Arsia Mons, Mars. *Earth and Planetary Science Letters*, *458*, 170–178. https://doi.org/10.1016/j.epsl.2016.10.040

Righter, K., Dyar, M. D., Delaney, J. S., Vennemann, T. W., Hervig, R. L., & King, P. L. (2002). Correlations of octahedral cations with OH, O_2, Cl, and F in biotite from volcanic rocks and xenoliths. *American Mineralogist*, *87*(1), 142–153. https://doi.org/10.2138/am-2002-0115

Righter, K., Pando, K., & Danielson, L. R. (2009). Experimental evidence for sulfur-rich Martian magmas: Implications for volcanism and surficial sulfur sources. *Earth and Planetary Science Letters*, *288*(1-2), 235–243. https://doi.org/10.1016/j.epsl.2009.09.027

Robie, R. A., Hemingway, S., & Fisher, J. R. (1979). Thermodynamic properties of minerals and related substances at 298.15 K and 1 Bar (105 Pascals) pressure and at higher temperatures. *U.S. Geological Survey Bulletin*, *1452*, 464. https://doi.org/10.3133/b2131

Salazar, J. S., Perez, L., de Abril, O., Truong Phuoc, L., Ihiawakrim, D., Vazquez, M., et al. (2011). Magnetic iron oxide nanoparticles in 10– 40 nm range: Composition in terms of magnetite/maghemite ratio and effect on the magnetic properties. *Chemistry of Materials*, *23*(6), 1379–1386. https://doi.org/10.1021/cm103188a

Santos, A. R., Agee, C. B., McCubbin, F. M., Shearer, C. K., Burger, P. V., Tartese, R., & Anand, M. (2015). Petrology of igneous clasts in Northwest Africa 7034: Implications for the petrologic diversity of the Martian crust. *Geochimica et Cosmochimica Acta*, *157*, 56–85. https://doi.org/10.1016/j.gca.2015.02.023

Savijärvi, H. I., Harri, A. M., & Kemppinen, O. (2015). Mars Science Laboratory diurnal moisture observations and column simulations. *Journal of Geophysical Research: Planets*, *120*, 1011–1021. https://doi.org/10.1002/2014JE004732

Schmidt, M. E., Schrader, C. M., & McCoy, T. J. (2013). The primary fO_2 of basalts examined by the Spirit rover in Gusev Crater, Mars: Evidence for multiple redox states in the Martian interior. *Earth and Planetary Science Letters*, *384*, 198–208. https://doi.org/10.1016/j.epsl.2013.10.005

Schuttlefield, J. D., Sambur, J. B., Gelwicks, M., Eggleston, C. M., & Parkinson, B. A. (2011). Photooxidation of chloride by oxide minerals: Implications for perchlorate on Mars. *Journal of American Chemical Society*, *133*, 17,521–17,523. https://doi.org/10.1021/ja2064878

Settle, M. (1979). Formation and deposition of volcanic sulfate aerosols on Mars. *Journal of Geophysical Research*, *84*, 8343–8354. https://doi.org/10.1029/JB084iB14p08343

Shinohara H. (2008). Excess degassing from volcanoes and its role on eruptive and intrusive activity. *Reviews in Geophysics*, *46*, RG4005

Sklute, E. C., Rogers, A. D., Gregerson, J. C., Jensen, H. B., Reeder, R. J., & Dyar, M. D. (2018). Amorphous salts formed from rapid dehydration of multicomponent chloride and ferric sulfate brines: Implications for Mars. *Icarus*, *302*, 285–295. https://doi.org/10.1016/j.icarus.2017.11.018

Stoffregen, R. E. (1987). Genesis of acid-sulfate alteration and Au-Cu-Ag mineralization at Summitville, Colorado. *Economic Geology*, *82*(6), 1575–1591. https://doi.org/10.2113/gsecongeo.82.6.1575

Symonds, R. B., & Reed, M. H. (1993). Calculation of multicomponent chemical equilibria in gas-solid-liquid systems: Calculation methods, thermochemical data, and applications to studies of high-temperature volcanic gases with examples from Mt. St. Helens. *American Journal of Science*, *293*. https://doi.org/10.2475/ajs.293.8.758

Symonds, R. B., Rose, W. I., Bluth, G. J., & Gerlach, T. M. (1994). Volcanic-gas studies; methods, results, and applications. *Reviews in Mineralogy and Geochemistry*, *30*(1), 1–66.

Taran, Y. A., Hedenquist, J. W., Korzhinsky, M. A., Tkachenko, S. I., & Shmulovich, K. I. (1995). Geochemistry of magmatic gases from Kudryavy volcano, Iturup, Kuril Islands. *Geochimica et Cosmochmica Acta*, *59*(9), 1749–1761. https://doi.org/10.1016/0016-7037(95)00079-F

Torrent, J., & Barrón, V. (2000). Key role of phosphorus in the formation of the iron oxides in Mars soils? *Icarus*, *145*, 645–647. https://doi.org/10.1006/icar.2000.6408

Ustunisik, G., Nekvasil, H., & Lindsley, D. (2011). Differential degassing of H_2O, Cl, F, and S: Potential effects on lunar apatite. *American Mineralogist*, *96*, 1650–1653. https://doi.org/10.2138/am.2011.3851

Ustunisik, G., Nekvasil, H., Lindsley, D. H., & McCubbin, F. M. (2015). Degassing pathways of Cl-, F-, H-, and S-bearing magmas near the lunar surface: Implications for the composition and Cl isotopic values of lunar apatite. *American Mineralogist*, *100*, 1717–1727. https://doi.org/10.2138/am-2015-4883

Vaniman, D. T., Bish, D. L., Ming, D. W., Bristow, T. F., Morris, R. V., Blake, D. F., et al. (2014). Mineralogy of a mudstone at Yellowknife Bay, Gale Crater, Mars. *Science*, *343*(6169), 1243480. https://doi.org/10.1126/science.1243480

Vaucher, J., Baratoux, D., Mangold, N., Pinet, P., Kurita, K., & Grégoire, M. (2009). The volcanic history of central Elysium Planitia: Implications for Martian magmatism. *Icarus*, *204*, 418–442. https://doi.org/10.1016/j.icarus.2009.06.032

Wadhwa, M. (2008). Redox conditions on small bodies, the Moon and Mars. *Reviews in Mineralogy and Geochemistry*, *68*, 493–510. https://doi.org/10.2138/rmg.2008.68.17

Wallace, P. J. (2001). Volcanic SO_2 emissions and the abundance and distribution of exsolved gas in magma bodies. *Journal of Volcanology and Geothermal Research*, *108*, 85–106. https://doi.org/10.1016/S0377-0273(00)00279-1

Wänke, H., Brückner, J., Dreibus, G., Rieder, R., & Ryabchikov, I. (2001). Chemical composition of rocks and soils at the Pathfinder site. *Space Science Reviews*, *96*(1-4), 317–330. https://doi.org/10.1023/A:1011961725645

Wang, A., Yan, W., Houghton, J., Jolliff, B. L.,& Wang, K. (2019). Plasma Chemistry induced by martian dust storms and dust devils. 50th Lunar and Planetary Science Conference , *Abstract #2031*.

Waters, L. E., & Lange, R. A. (2016). No effect of H_2O degassing on the oxidation state of magmatic liquids. *Earth and Planetary Science Letters*, *447*, 48–59. https://doi.org/10.1016/j.epsl.2016.04.030

Webster, A. H., & Bright, N. F. (1961). The system iron–titanium–oxygen at 1200°C and oxygen partial pressures between 1 Atm. and 2×10^{-14} Atm. *Journal of the American Ceramic Society*, *44*, 110–116. https://doi.org/10.1111/j.1151-2916.1961.tb13723.x

Wilson, E. H., Atreya, S. K., Kaiser, R. I., & Mahaffy, P. R. (2016). Perchlorate formation on Mars through surface radiolysis-initiated atmospheric chemistry: A potential mechanism. *Journal of Geophysical Research: Planets*, *121*, 1472–1487. https://doi.org/10.1002/2016JE005078

Wilson, L., & Head, J. W. (2007). Explosive volcanic eruptions on Mars: Tephra and accretionary lapilli formation, dispersal and recognition in the geologic record. *Journal of Volcanology and Geothermal Research*, *163*(1-4), 83–97. https://doi.org/10.1016/j.jvolgeores.2007.03.007

Yang, X. J., Xu, X. M., Xu, J., & Han, Y. F. (2013). Iron oxychloride (FeOCl): an efficient Fenton-like catalyst for producing hydroxyl radicals in degradation of organic contaminants. *Journal of the American Chemical Society*, *135*, 16,058–16,061. https://doi.org/10.1021/ja409130c

Yant, M., Rogers, A. D., Nekvasil, H., Zhao, Y. S., & Bristow, T. (2016). Spectral characterization of acid weathering products on Martian basaltic glass. *Journal of Geophysical Research: Planets*, *121*, 516–541. https://doi.org/10.1002/2015JE004969

Yudovskaya, M. A., Tessalina, S., Distler, V. V., Chaplygin, I. V., Chugaev, A. V., & Dikov, Y. P. (2008). Behavior of highly-siderophile elements during magma degassing: A case study at the Kudryavy volcano. *Chemical Geology*, *248*, 318–341. https://doi.org/10.1016/j.chemgeo.2007.12.008

Zelenski, M. E., Fischer, T. P., De Moor, J. M., Marty, B., Zimmermann, L., Ayalew, D., & Karandashev, V. K. (2013). Trace elements in the gas emissions from the Erta Ale volcano, Afar, Ethiopia. *Chemical Geology*, *357*, 95–116. https://doi.org/10.1016/j.chemgeo.2013.08.022

Zent, A. P., & McKay, C. P. (1994). The chemical reactivity of the Martian soil and implications for future missions. *Icarus*, *108*(1), 146–157. https://doi.org/10.1006/icar.1994.1047

Zhang, J., Liu, G., Wang, P., & Liu, S. (2017). Facile synthesis of FeOCl/iron hydroxide hybrid nanosheets: enhanced catalytic activity as a Fenton-like catalyst. *New Journal of Chemistry*, *41*(18), 10,339–10,346. https://doi.org/10.1039/C7NJ01993A

Zolotov, M. Y., & Shock, E. L. (2005). Formation of jarosite-bearing deposits through aqueous oxidation of pyrite at Meridiani Planum, Mars. *Geophysical Research Letters*, *32*, L21203. https://doi.org/10.1029/2005GL024253